PL-TR-94-2283

STATISTICAL DISCRIMINATION STUDIES FOR NUCLEAR TEST VERIFICATION

Robert H. Shumway
Allan D.R. McQuarrie

University of California
Division of Statistics
Davis, CA 95616

31 December 1994

Final Report
1 July 1991 - 31 December 1994

Approved for public release; distribution unlimited

PHILLIPS LABORATORY
Directorate of Geophysics
AIR FORCE MATERIEL COMMAND
HANSCOM AIR FORCE BASE, MA 01731-3010

This technical report has been reviewed and is approved for publication.

JAMES F. LEWKOWICZ
Contract Manager
Earth Sciences Division

JAMES F. LEWKOWICZ
Director
Earth Sciences Division

This report has been reviewed by the ESC Public Affairs Office (PA) and is releasable to the National Technical Information Service (NTIS).

Qualified requestors may obtain additional copies from the Defense Technical Information Center. All others should apply to the National Technical Information Service.

If your address has changed, or if you wish to be removed from the mailing list, or if the addressee is no longer employed by your organization, please notify PL/IM, 29 Randolph Road, Hanscom AFB, MA 01731-3010. This will assist us in maintaining a current mailing list.

Do not return copies of this report unless contractual obligations or notices on a specific document requires that it be returned.

REPORT DOCUMENTATION PAGE

Form Approved
OMB No. 0704-0188

1. AGENCY USE ONLY (Leave blank)	2. REPORT DATE	3. REPORT TYPE AND DATES COVERED
	December 31, 1994	Final 1 July 91 - 31 December 94

4. TITLE AND SUBTITLE

Statistical Discrimination Studies for Nuclear Test Verification

5. FUNDING NUMBERS

F19628-91-K-0033
PE 69120C
PR T121
TA TC WU AB

6. AUTHOR(S)

Robert H. Shumway
Allan D.R. McQuarrie

7. PERFORMING ORGANIZATION NAME(S) AND ADDRESS(ES)

Division of Statistics
University of California
Davis, CA 95616

8. PERFORMING ORGANIZATION REPORT NUMBER

Division of Statistics
Technical Report #304

9. SPONSORING/MONITORING AGENCY NAME(S) AND ADDRESS(ES)

Phillips Laboratory
29 Randolph Road
Hanscom AFB MA 01731-3010

Contract Manager: James Lewkowicz/GPE

10. SPONSORING/MONITORING AGENCY REPORT NUMBER

PL-TR-94-2283

11. SUPPLEMENTARY NOTES

12a. DISTRIBUTION/AVAILABILITY STATEMENT

Approved for public release; distribution unlimited

12b. DISTRIBUTION CODE

13. ABSTRACT *(Maximum 200 words)*

Robust statistical approaches to the problem of discriminating between regional earthquakes and explosions are developed. We compare linear discriminant analysis using descriptive features like amplitude and spectral ratios with signal discrimination techniques using the original signal waveforms and spectral approximations to the log likelihood function. Robust information theoretic techniques are proposed and all methods are applied to 8 earthquakes and 8 mining explosions in Scandinavia and to an event from Novaya Zemlya of unknown origin. It is noted that signal discrimination approaches based on discrimination information and Renyi entropy perform better in the test sample than conventional methods based on spectral ratios involving the P and S phases.

Two techniques for identifying the ripple-firing pattern for typical mining explosions are proposed and shown to work well on simulated data and on several Scandinavian earthquakes and explosions. We use both cepstral analysis in the frequency domain and a time domain method based on the autocorrelation and partial autocorrelation functions. The proposed approach strips off underlying smooth spectral and seasonal spectral components corresponding to the echo pattern induced by two simple ripple-fired models. For two mining explosions, a pattern is identified whereas for two earthquakes, no pattern is evident.

14. SUBJECT TERMS	15. NUMBER OF PAGES
Earthquakes and explosions, classification, signal discrimination, spectra, information theory, cepstrum, echo detection, ARMA models.	56
	16. PRICE CODE

17. SECURITY CLASSIFICATION OF REPORT	18. SECURITY CLASSIFICATION OF THIS PAGE	19. SECURITY CLASSIFICATION OF ABSTRACT	20. LIMITATION OF ABSTRACT
Unclassified	Unclassified	Unclassified	UL

TABLE OF CONTENTS

Part 1: Figures

Part 2: Figures

PART 1: STATISTICAL APPROACHES TO SEISMIC DISCRIMINATION

1.1 General Approaches to Discrimination

Conventional methods for discriminating between earthquakes and explosions at regional distances have concentrated on extracting specific features from the waveforms of the two arrival phases seen on the seismic record, denoted in this report by P and S. The specific features usually considered are amplitude ratios, measures of waveform complexity or various kinds of spectral ratios, suggesting that the main characterization of the differences between earthquakes and explosions can be reduced to comparing differences between the amplitude ratios or the spectral ratios of the two arrival phases. For purposes of discussion, we will term this approach the *feature extraction* approach. The variations on the above theme seem to change depending on the author and on the general region within which the discrimination study is done. The features may then combined using an optimal statistical procedure that assumes multivariate normality for the extracted feature vector and maximizes the probability of detecting an explosion for a fixed specified rate of false alarms.

An alternate approach, based on classical signal discrimination methodology, is to consider the two P and S waveforms as the underlying phenomena rather than the somewhat arbitrarily extracted features discussed above. The two waveforms are then modeled as general zero-mean stochastic processes with given unequal covariance functions and density functions based on the multivariate normal assumption. The same optimality criterion as above is applied to the underlying waveforms. We shall term this the *waveform discrimination* approach. This approach has the advantage (or disadvantage, depending on one's point of view) of eliminating the arbitrary step that decides in advance that certain extracted features are optimal and lets the statistical model dictate the method for combining the elements of the underlying signal waveforms. Modifications that are robust to departures from the above assumptions can be made using information theoretic measures.

It is natural and expected that seismologists are more comfortable with the feature extraction approach (Blandford, 1993, Dysart and Pulli, 1990, Fisk et al, 1993, Richards et al, 1993, Ryall, 1993, Taylor et al, 1989, Booker and Mitronovas, 1964) and that engineers and statisticians, who may lack the requisite geophysical knowledge and intuition for extracting reasonable features, should prefer the signal discrimination approach (Cavanaugh et al, 1993, Dargahi-Noubary and Laycock, 1981, Liggett, 1971, Shumway, 1982, 1983, Shumway and Unger, 1974, Shumway and Blandford, 1974, Zhang and Taniguchi,

1993, 1994). Happily, the final results of both procedures depend upon the spectra of the two phases and the two methods seem to yield somewhat similar results when applied to sample earthquakes and explosions.

The organization of Part 1 of this report is to first discuss the statistical approaches to discrimination that hold regardless of whether the underlying elements are the extracted features or the root waveforms. This is followed by a more specific discussion of the two approaches with applications to a population of eight earthquakes, eight mining explosions in Scandinavia and the Novaya Zemlya event (see Ryall, 1993) of unknown origin. The performance of the two approaches is compared on the common events and for the new event of unknown origin; it is shown that a robust modification to the waveform discriminator performs best in this particular situation.

As demonstration data, we use a subset of stations recording 8 earthquakes and 8 explosions in Scandinavia from the arrays NORESS, ARCESS and FINESS as described in Blandford [4] (see also Cavanaugh et al (1993) for more details). According to Blandford, "The events were selected with consideration for having sufficient S/N at single elements so that all phases could be clearly seen on all components of a single instrument $\cdots$". All events chosen by Blandford were on or near land and were distributed uniformly over Scandinavia to minimize the possibility that discriminators might be keying on location or land-sea differences. Figure 1 shows portions of a typical earthquake and explosion (sampled at 20 Hz), along with the unknown Novaya Zemyla event of 31 December, 1992. The earthquake exhibits the often observed lower amplitude of the first arrival P phase as compared to the later S phase. The explosions ranged from magnitude 2.13 to 2.19 with the earthquakes in the range 2.74 to 4.40. The Novaya Zemyla event was of magnitude 2.5. For computations, we did not identify specific phases through velocity computations but simply chose fairly broad (25 second) windows that seemed to include the major portions of the P and S phases.

1.2 Statistical Optimality

The problem of discriminating between earthquakes and explosions is an example of a general pattern recognition problem in statistics where we wish to classify an observed vector $\mathbf{x} = (x_1, x_2, \ldots, x_p)'$ consisting of p features or of a p dimensional waveform into one of two populations, denoted in general by H_1: Earthquake and H_2: Explosion. Key statistical properties of any classification procedure are the false alarm rate $P(2|1)$, defined as the probability of accepting the explosion hypothesis, given that the event is an

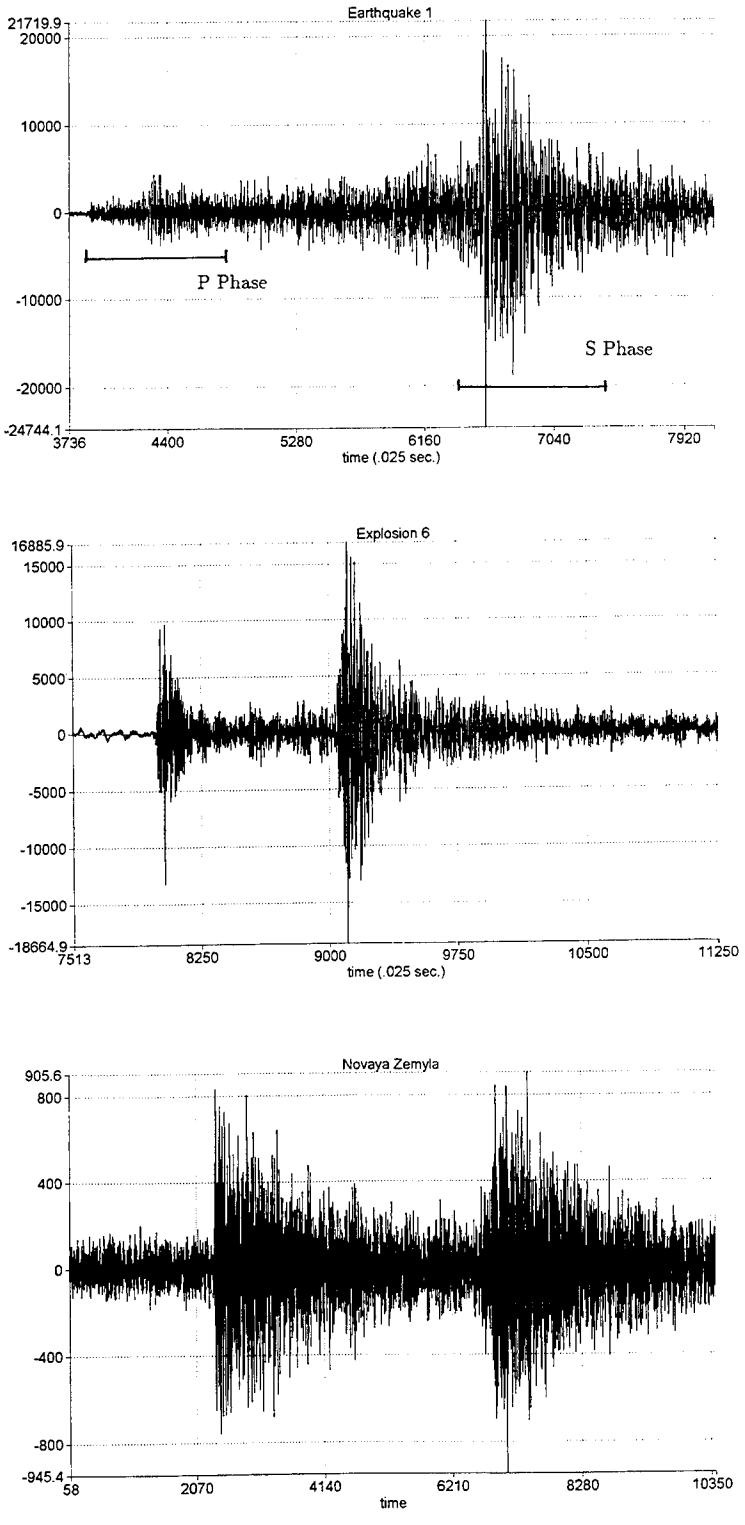

Figure 1: A Typical Earthquake Compared With a Typical Explosion and the Novaya Zemyla Event.

earthquake and $P(2|2)$, the probability of detecting an explosion. The seismic discrimination problem is expressed then as one of distinguishing between two hypotheses and fits nicely into classical signal discrimination and detection theory. Detailed treatments can be found in many places; we mention Anderson (1971) for an exposition of the background statistics and Shumway (1982), (1988) for extensions of these ideas to time series analysis.

To begin, suppose that we denote the probability densities of the observed vector under the two hypotheses by $p_1(\mathbf{x})$ and $p_2(\mathbf{x})$ respectively. It is well known that the best rule, in the sense of maximizing the detection probability for a fixed false alarm rate, results from classifying $\mathbf{x}$ into H_1 when

$$\frac{p_1(\mathbf{x})}{p_2(\mathbf{x})} > K$$

and into H_2 otherwise. Simple rules result when one further specializes by requiring that the densities $p_1(\mathbf{x})$ and $p_2(\mathbf{x})$ correspond to multivariate normal distributions. One chooses the constant to have a specified false alarm rate or as the ratio of prior probabilities of H_2 and H_1 in the Bayesian case. It is plausible to assume that the two populations differ only in the mean vectors when one is looking at extracted features and differ only in the covariance structure when one is looking at waveforms.

For the case where only the means μ_1 and μ_2 are different and the covariance matrices R_1 and R_2 take some common value R, the rule given above reduces to choosing H_1 whenever $c_2 > c_2$ and choosing H_2 otherwise, where

$$c_j = \mu_j' \, R^{-1}\mathbf{x} - \frac{1}{2} \, \mu_j' \, R^{-1}\mu_j, \tag{1.1}$$

$j = 1, 2$, and we assume $K = 1$ corresponding to equal prior probabilities for H_1 and H_2. This linear discriminant function is easy to apply and leads to comparing two single numbers in order to make a decision. If the mean vectors and covariance matrix are known, the distributional properties of the linear function can be evaluated explicitly to give predicted values for the performance measures $P(2|1)$ and $P(2|2)$. We temporarily defer discussion of what to do when this is not the case.

When the means $\mu_1 = \mu_2 = 0$ are the same but the covariance functions R_1 and R_2 are different, the test procedure reduces to accepting H_1 when $d_1 > d_2$ and H_2 otherwise, where

$$d_j = -\frac{1}{2} \, \log|R_j| - \frac{1}{2} \, \mathbf{x}' R_j^{-1}\mathbf{x}, \tag{1.2}$$

$j = 1, 2$, which shows that the criterion in this case reduces to a *quadratic discriminant function.* Even if the covariance matrices are known, the distribution of the test statistic is intractable and the performance measures are extremely difficult to evaluate.

Both procedures given above require estimators for the means and covariance matrices if they cannot assumed to be known. In the seismic case, this means that small training samples, often highly dependent on source and array parameters, must be used in order to develop sample mean vectors and covariance matrices. The performance characteristics of the linear and quadratic discriminant functions become even more uncertain under these conditions and we need to use resampling techniques to estimate the performance measures $P(2|1)$ and $P(2|2)$. A commonly used resampling technique that produces reasonable estimators is to compute the *holdout classification function* proposed by Lachenbruch and Mickey (1968). In this procedure, one "holds out" the observation to be classified when estimating the discriminant functions (1.1) and (1.2). That is, the sample mean and covariance matrices are computed for the training sample with the observation to be classified held out. The overall sample error rates and detection probabilities are then better estimators for the true population values.

An alternative but closely related proposal by Fisk et al (1993) derives the likelihood ratio criterion for testing whether the held out observation belongs to the earthquake or explosion population (see also Anderson, 1971). The performance measures are then evaluated by resampling the likelihood ratio test statistic using the bootstrap. The authors have shown in simulations that this procedure also produces reasonable estimators for the performance measures. We do not discuss this interesting proposal further here and have not replicated this approach using our data.

It is clear that the above procedures depend more or less on a number of assumptions. For the mean differences approach, applied often in feature extraction, the computations are fairly simple because the dimensionality is small. The Gaussian assumption is needed for the linear function to be optimal and this is almost always plausible if one transforms using logarithms. Equality of the two covariance matrices is assumed and generally can be satisfied by using ratios of features from the P and S phases. The effects of small samples and other departures are mitigated by using a resampling procedure.

The waveform discrimination approach introduces additional computational difficulties because of the large dimensions of the signal vectors. This is circumvented by using spectral approximations for the densities $p_1(\mathbf{x})$ and $p_2(\mathbf{x})$ proposed first by Whittle (1954). Departures from the Gaussian assumption are not particularly important since the approximations involve sums which converge to Gaussian distributions rather quickly and because recent analyses by Zhang and Taniguchi (1993), (1994) have shown that modifications to the classical approximations are robust towards such departures. Even perturbations in the spectra can be tolerated for the test statistics used in Section 4. Again, resampling

techniques are necessary in order to provide reasonable estimates for the false alarm and signal detection probabilities.

1.3 Feature Extraction

In order to develop a linear discriminant function for extracting features using (1.1), we need to determine the ingredients for the feature vector $\mathbf{x} = (x_1, x_2, \ldots, x_p)'$. An early application of this idea to discriminating at teleseismic distances was by Booker and Mitronovas (1964) who used surface wave and body wave magnitudes as components. In the case of regional data, numerous investigators have pointed out that the logarithms of $P_g/L_g(P/S)$ amplitude ratios tend to be lower for earthquakes than for explosions. The top panel in Figure 2 shows the values of $-\log P/S$ amplitudes for the 8 earthquakes and explosions and for Novaya Zemyla. It is clear that there is reasonable separation and that the Novaya Zemlya event falls with the explosion group. Considerable past effort has been expended on spectral ratios involving the P and S groups. Bennett and Murphy (1986) note that for western U.S. events, earthquake L_g spectra contained more high frequencies, and that the ratio of the logarithms of low frequency (.5-1 Hz) L_g to higher frequency L_g (2-4 Hz) tend to be larger for explosions. Taylor et al (1989) also use this ratio over the frequency bands (1-2 Hz) and (6-8 Hz) and extended the consideration to the P_g phase. Dysart and Pulli (1990) have also considered various spectral ratios P/S for Scandinavian events and have developed nonlinear neural networks as an alternative to simple linear combinations of features for discrimination. They note that the P/S spectral ratios are generally higher for explosions than for earthquakes. Finally, Richards et al (1993) note that for eastern U.S. events the ratios of P_g to L_g spectra are generally higher for explosions. For our particular feature extraction example using the Scandinavian earthquakes and explosions, we consider incorporating P and S amplitudes and P and S spectra over relatively broad low and high frequency bands (0-8 Hz, 6-12 Hz). The frequency ranges were not exactly comparable to those used in the literature (.5-1Hz, 2-4 Hz in Bennett and Murphy, 1986, 1-2 Hz, 6-8 Hz in Taylor et al, 1989, 2-5 Hz, 5-10 Hz, 10-20 Hz in Dysart and Pulli, 1990, 5-25(5) Hz in Richards et al, 1993) but were chosen by visually inspecting the separate spectra and the average earthquake and explosion spectra. Taking logarithms improves the approximation to normality required for application of (1.1). We also used the ratios of P to S components $(-\log P/S)$ in order to equalize the covariance matrices of the earthquake and explosion populations. Hence, we ended with three basic components representing amplitude ratios and two spectral ratios, say $\mathbf{x} = (x_1, x_2, x_3)'$ for application in the linear discriminant function (1). Figure 2 shows the separation for the populations

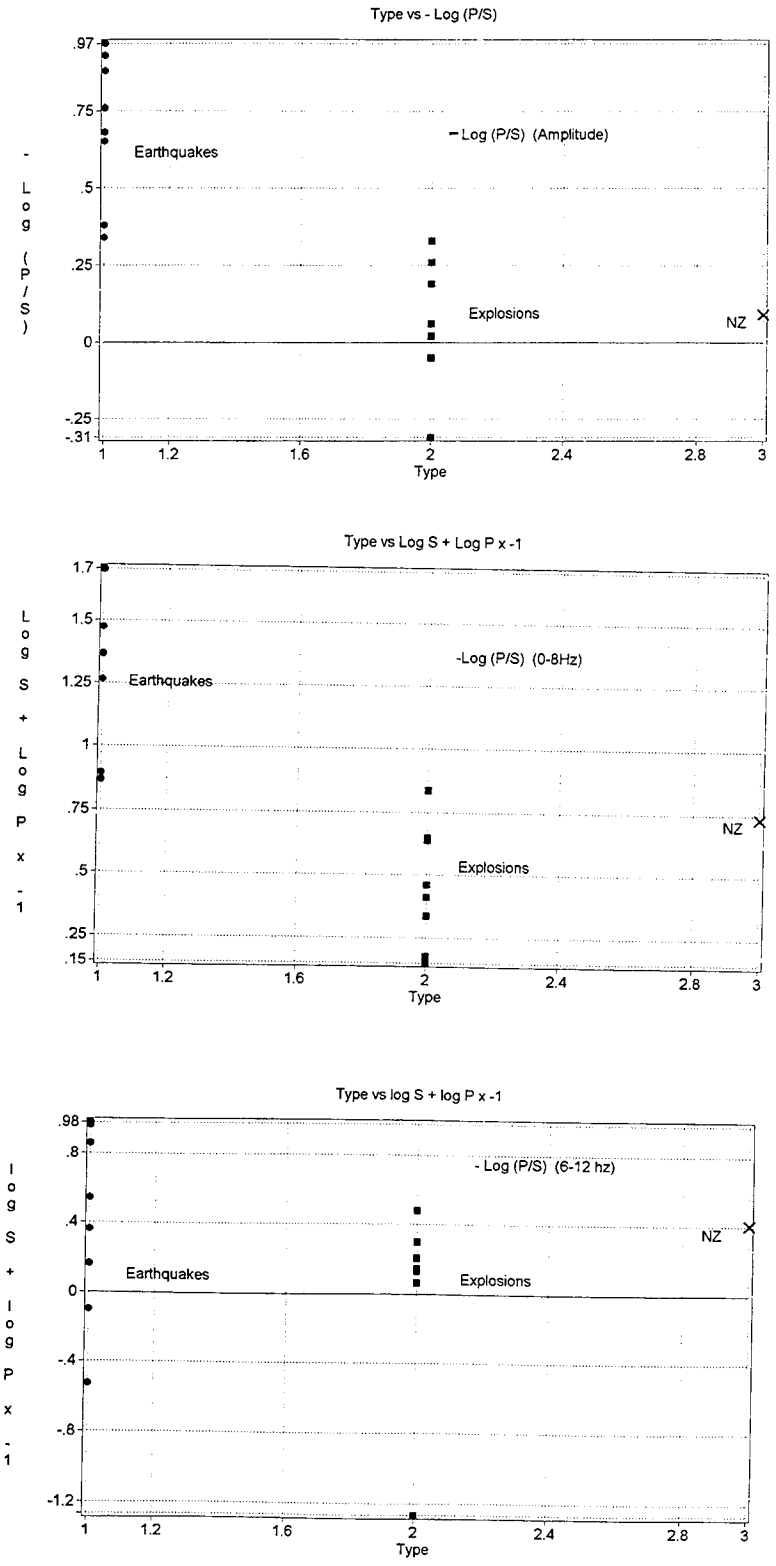

Figure 2: Separation Achieved for Earthquakes and Explosions Using Log Amplitude Ratios (Top Panel) Low Frequency (0-8Hz) (Middle Panel) and High Frequency (6- 12 Hz) (Bottom Panel) Spectral Ratios.

of 8 earthquakes and explosions spectral ratios over the low frequency (0-8 Hz) and high frequency (6-12 Hz) bands. Note the reasonable separation for the low frequency band and the generally poor performance over the high frequency band.

We applied the linear discriminant function using various combinations of the amplitude and spectral ratios to the populations of 8 earthquakes and 8 mining explosions. Table 1 shows the results using the holdout classification procedure. That is, each classification is made using a learning population not containing the event to be classified. The two columns are the number of misclassified earthquakes (as explosions) and explosions (as earthquakes) respectively. Dividing the entries by 8 would give estimators for $P(2|1)$ and $P(1|2)$ respectively. Results using the *minimum discrimination information* and *α-entropy* measures described in the next section are also included for purposes of comparison.

Table 1: Misclassifications (Holdout)

Method	*EQ*	*EXP*
Amplitude Ratio	1	1
Amplitude-Low Frequency Spectral Ratio	1	2
Low Frequency and High Frequency Spectral Ratios	0	1
Amplitude, Low and High Frequency Spectral Ratios	0	1
Minimum Discrimination Information	0	1
α-Entropy	0	0

It is clear that the amplitude and low frequency spectral ratios include essentially the same information, so that combining them does not work well. For comparison purposes, it appears that the log amplitude ratios work best as a single discriminator and that the two spectral ratios work as the best pair. The problem event is always the first explosion that gets classified as an earthquake in the holdout procedure. Using amplitude ratios, the posterior probability that the first explosion is an earthquake is .88; using the two spectral ratios, it is .97. The event of unknown origin at Novaya Zemyla is classified as an explosion with high probability (.98, 1.00) by the two procedures.

1.4 Waveform Discrimination

For the waveform approach to classification we regard the entire time realization as the signal of interest. Because of the separate P and S phases that always seem to be present, it is convenient to think of them as a bivariate process, so that there are two signal vectors,

each composed of a window (25 seconds here) of one of the phases. It is fairly evident that, in the case of regional events, the signals may be regarded as zero mean processes and that the differences between signals from earthquakes and explosions might be due exclusively to differences between the spectra. The two P and S signals are uncorrelated and incoherent (this was checked for the sample of 8 earthquakes and explosions in this study) and hence can be regarded as uncorrelated processes with unequal P and S spectra for earthquakes and explosions.

In order to apply the quadratic discriminant function, which would be appropriate for distinguishing between the earthquake and explosion processes, we need a method for computing the discriminant function (1.2). Long signals make this computation difficult and it is conventional to apply an approximate form due to Whittle [22], say

$$d_{j\cdot} = -\frac{1}{2}\sum_{k=0}^{T-1}\left\{\log f_{j\cdot}(\nu_k) + \frac{|X_{\cdot}(k)|^2}{f_{j\cdot}(\nu_k)}\right\}, \tag{1.3}$$

where we replace $\cdot$ by P or S depending on the phase to be considered, $X_{\cdot}(k)$ is the discrete Fourier transform of the data $x_{t\cdot}$ and $f_{j\cdot}(\nu_k)$ denotes the spectrum for phase $\cdot$ under hypothesis H_j. The frequencies are of the form $\nu_k = k/T, k = 0, \ldots, T-1$. Liggett (1971) established that the scaled (by 1/T) difference between (1.3) and (1.2) converges almost surely to zero. The optimal statistic for testing whether the sampled bivariate series is from H_1: Earthquake or from H_2:Explosion is given by

$$Q = (d_{1P} - d_{2P}) + (d_{1S} - d_{2S}), \tag{1.4}$$

where we accept H_1 if $Q > 0$ and H_2 if $Q \leq 0$. The procedure for discrimination using a single waveform and (3) is by now well established in the statistical literature, having been applied by Alagon (1989), Cavanaugh et al (1993), Dargahi-Noubaryand Laycock (1981), Shumway and Unger (1974), Shumway and Blandford (1974) and Shumway (1982), (1988) to seismic signal discrimination problems.

It is useful to give an information theoretic interpretation to the test given above since this exercise leads to two new test procedures that turn out to be robust to departures from assumptions. Kullback (1959) has developed the minimum discrimination information (MDI) criterion as a means for classifying a new observation into H_1 or H_2. Pinsker (1964) derived the limiting form of the discrimination information under the assumption that one has two Gaussian processes differing only in the spectra. For the MDI criterion, one compares the discrepancy of a spectral estimator computed from the sample realization

$x_{t\cdot}$, say $f_{T\cdot}(\nu_k)$, with $f_{1\cdot}(\nu_k)$ and $f_{2\cdot}(\nu_k)$ using

$$I(f_{T\cdot}, f_{j\cdot}) = \frac{1}{2}\sum_{k=0}^{T-1}\left\{\frac{f_{T\cdot}(\nu_k)}{f_{j\cdot}(\nu_k)} - \log\frac{f_{T\cdot}(\nu_k)}{f_{j\cdot}(\nu_k)} - 1\right\}. \tag{1.5}$$

The above can be regarded as a measure of the match between the sample spectrum and the theoretical value $f_{j\cdot}(\nu_k)$ for $j = 1, \cdot = P, S$ earthquakes and $j = 2, \cdot = P, S$ explosions. A reasonable procedure would be to look at the difference

$$I(f_{1\cdot}, f_{2\cdot}; f_{T\cdot}) = I(f_{T\cdot}, f_{2\cdot}) - I(f_{T\cdot}, f_{1\cdot}), \tag{1.6}$$

between the matches to the two theoretical spectra. Since we want the discrepancy between the sample spectrum and the true density to be minimized, it is clear that we should accept H_1 when $I(f_{1\cdot}, f_{2\cdot}; f_{T\cdot}) \geq 0$ and accept H_2 otherwise. In terms of the overall criterion, expressed in terms of both phases we would choose H_1 (earthquake) when the sum of (6) over the $\cdot = S, \cdot = P$ exceeds 0 and accept H_2 (explosion) otherwise. Note that for $f_{T\cdot}(\nu_k) = |X_{\cdot}(k)|^2$, the periodogram estimator, the above criterion reduces exactly to the quadratic criterion defined in (1.3). Zhang and Taniguchi (1993) , (1994) have shown the asymptotic normality of the MDI criterion and that the misclassification errors converge to zero. They have also shown that the criterion is robust to departures from normality.

Zhang and Taniguchi have also suggested the Renyi α-*entropy*, $(0 < \alpha < 1)$ see Renyi (1961) as an alternative and show that it is robust to both non-Gaussian departures and peak contamination. Under this suggestion,define

$$e_\alpha(f_{j\cdot}, f_{T\cdot}) = \frac{1}{2}\sum_{k=0}^{T-1}\left\{\log\left(1 - \alpha + \alpha\frac{f_{j\cdot}(\nu_k)}{f_{T\cdot}(\nu_k)}\right) - \alpha\log\frac{f_{j\cdot}(\nu_k)}{f_{T\cdot}(\nu_k)}\right\}. \tag{1.7}$$

and accept H_1 when

$$B_\alpha(f_{1\cdot}, f_{2\cdot}; f_{T\cdot}) \geq 0,$$

where

$$B_\alpha(f_{1\cdot}, f_{2\cdot}; f_{T\cdot}) = e_\alpha(f_{2\cdot}, f_{T\cdot}) - e_\alpha(f_{1\cdot}, f_{T\cdot}) \tag{1.8}$$

In terms of the overall criterion involving both phases, we would again accept H_1 when the sum of (8) over $\cdot = P, \cdot = S$ exceeds 0.

In order to apply the discriminant functions defined above, we need to have estimators for the earthquake and explosion spectra, say $f_{1\cdot}(\nu)$ and $f_{2\cdot}(\nu)$. These can be taken as predefined values if no training sample is available or as the averages of the earthquake and

explosion spectra respectively if a training sample is available. We take the values here of the average earthquake and explosion spectra (see Cavanaugh et al, 1993). The spectra were computed for each series (no taper) over a fairly broad band (2 Hz) and then averaged separately for earthquakes and explosions. The event to be classified was held out of the averages. Note that the P and S components were scaled by dividing by the maximum of the P component. Figure 3 shows the spectra average earthquake and explosion P and S spectra for a fairly broad (2 Hz) bandwidth and for a somewhat more narrow bandwidth (.8 Hz). Note the nulls in the average explosion spectra indicating the possibility of delay-fired phenomena. We investigate this further in Part 2. For the quadratic and information theoretic detectors, small values of the theoretical spectra can cause potential distortions, so several cutoff frequencies (8 Hz, 12 Hz) and several bandwidths (.1 Hz, .8 Hz, 2 Hz) in (1.5) and (1.7) were tried; overall best performance seemed to be attained with a cutoff of about 8 Hz. The discriminants performed equally well over all three bandwidths and we chose 2 Hz as a final bandwidth.

Table 1 shows one misclassification (the first explosion again) for the discrimination information and no misclassifications for the *α-entropy* with $\alpha = .7$. Furthermore, the *α-entropy* shows excellent separation between the earthquake and explosion population as shown in Figure 4. The minimum discrimination information based on (1.5) and the optimal quadratic detector based on (1.7) both separated the populations as well but there was again one misclassification. Overall, the *α-entropy* yielded the largest separation of the two populations. Again, we see that the Novaya Zemyla event falls well within the explosion group.

1.5 Discussion

In Part 1, we have reviewed statistical procedures for discriminating between earthquakes and explosions that ensure that, for a set explosion false alarm rate, the detection probability will be maximized. These optimal statistical classification procedures turn out to be linear if extracted features based on amplitude and spectral characteristics of the P and S phases are used. Furthermore, the dimensionality of the classification function is usually relatively low. In the case of waveform discrimination, the dimensionality is rather high but the optimal procedures again turn out to be functionally dependent on the spectra of the P and S phases. Optimal discrimination procedures are therefore quadratic functions of the original waveforms and they reduce to computing functions that match these original waveforms to the group average using matching functions like (1.3), (1.5) and (1.7).

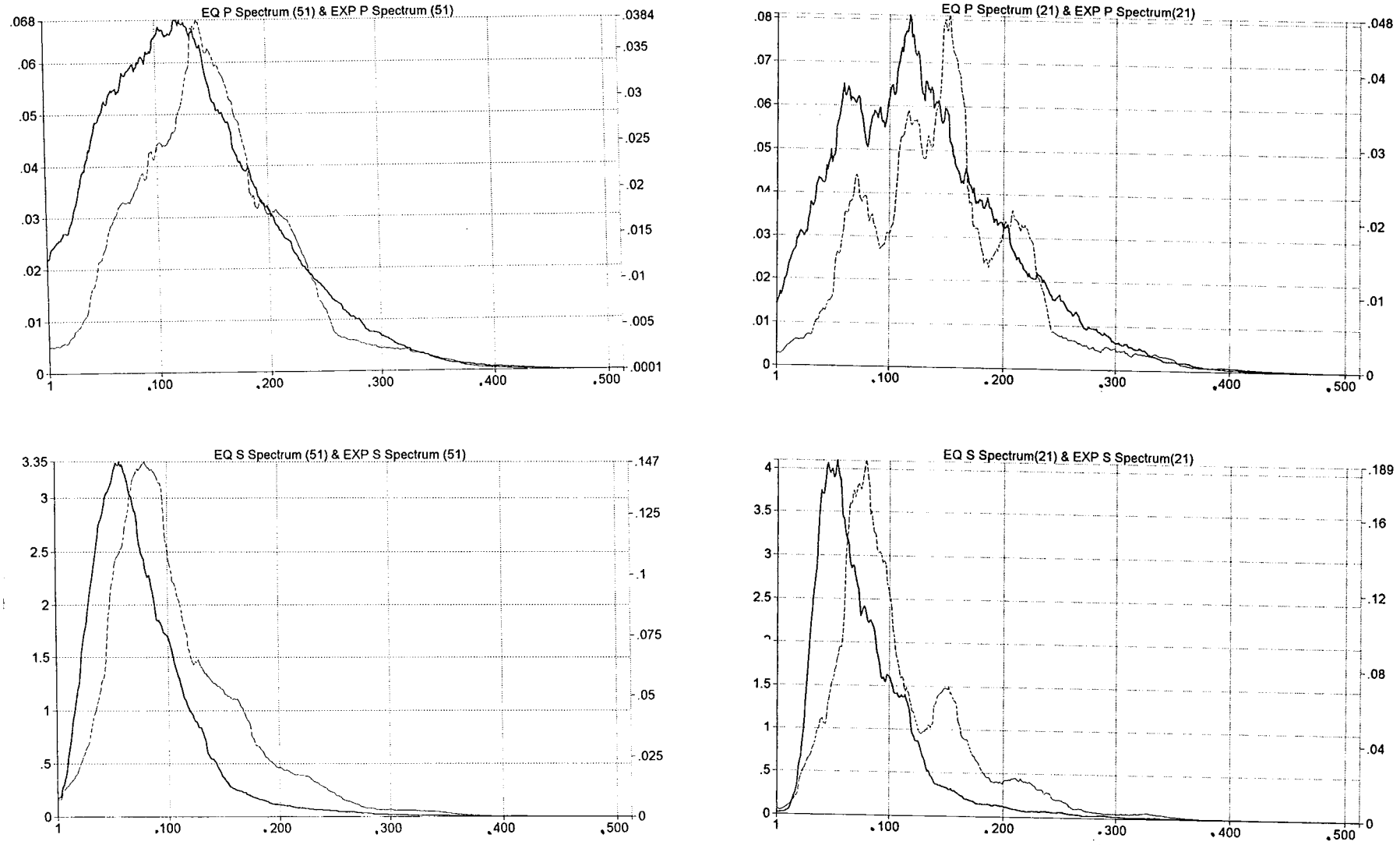

Figure 3: Average Earthquake and Explosion P and S Spectra Compared for Two Bandwidths (2 Hz, .8 Hz) Reading from left to right. The folding frequency of .5 cycles per point corresponds to 20 Hz.

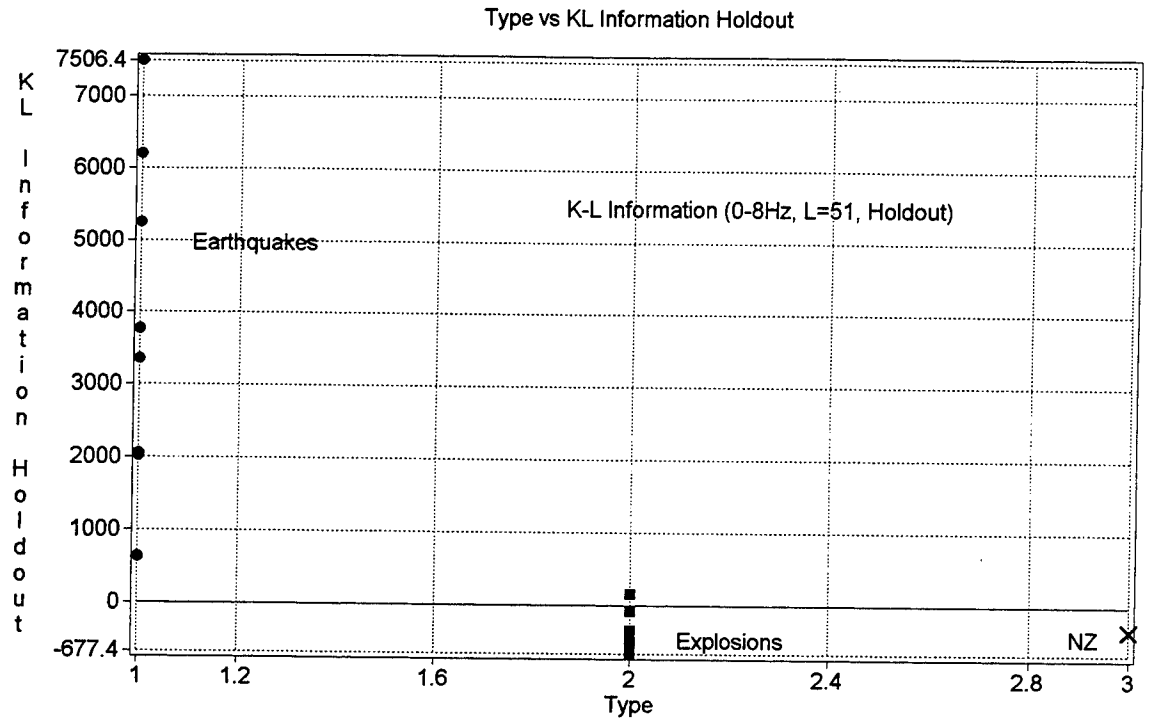

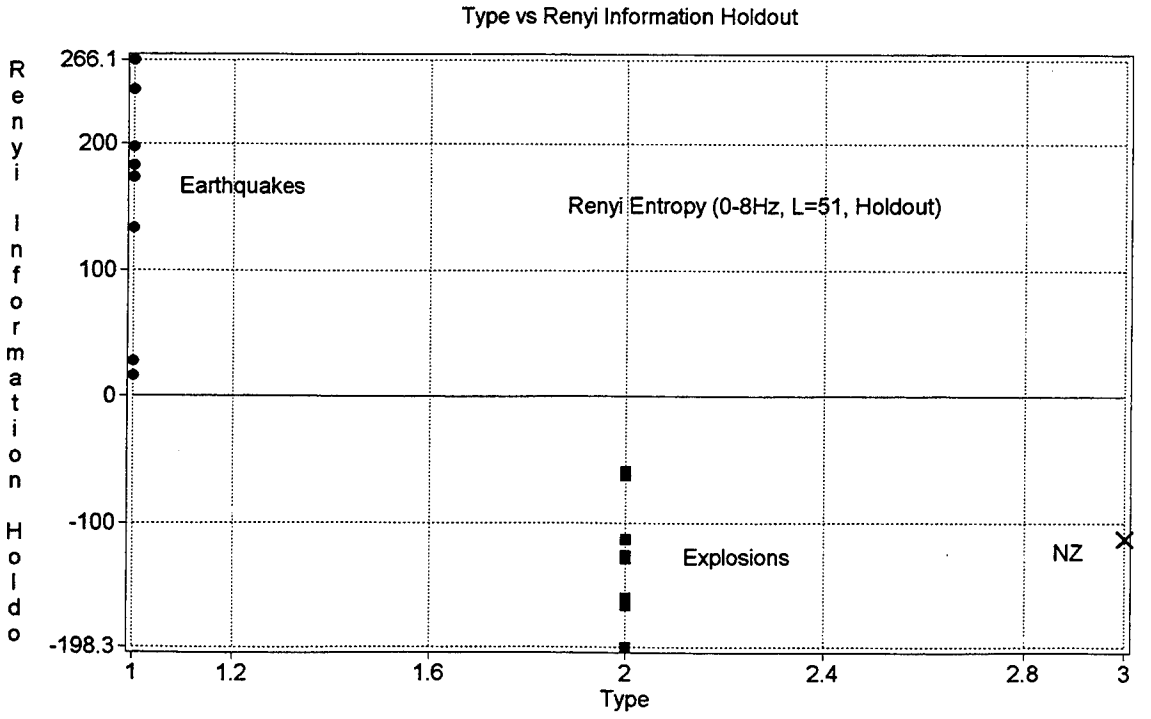

Figure 4: Separation Achieved for Information Theoretic Spectral Matching Measures. The top panel shows holdout values for the discrimination information whereas the bottom panel shows the values for the α-entropy.

An important consideration in any statistical discrimination procedure is the extent to which the particular features extracted or the signal waveforms tend to conform or fail to conform to underlying assumptions like multivariate normality that drive the theoretical derivations. Hence, for extracted features from the particular sample of Scandinavian earthquakes and explosions, we used logarithms and took ratios of components of the two separate P and S waveforms. For the waveform discrimination procedures, theoretical results of Zhang and Taniguchi (1993), (1994), available for the discrimination information and for the *α-entropy*, give credence to the claim that their overall performance is robust to departures from normality and to spectral peak contamination.

In the particular small sample of 8 earthquakes and 8 explosions and the unknown event from Novaya Zemyla, both the feature extraction and the waveform discrimination approaches performed well and all approaches classified the event from Novaya Zemyla with the mining explosion group. All methods except the *α-entropy* misclassified the first explosion as an earthquake. This decision was a strong preference of the feature extraction method but was on the borderline for the quadratic detector and for the discrimination information measures. The *α-entropy* still classified all events correctly in the holdout sample. These latter two observations tend to support the superiority of the optimal statistical classification methods as applied to the original waveforms.

1.6 References

Alagon, J. (1989). Spectral discrimination for two groups of time series. *J. Time Series Analysis*, **10**, 203-214.

Anderson, T.W. (1971). *An Introduction to Multivariate Statistical Analysis*, 2nd. ed. New York: Wiley.

Bennett, T.J. and J.R. Murphy (1986). Analysis of seismic discrimination capabilities using regional data from western U.S. events. *Bull. Seismolog. Soc. Amer.*, **76**, 1069-1086.

Blandford, R.R. (1993). Discrimination of earthquakes and explosions at regional distances using complexity. *AFTAC-TR-93-044*, HQ AFTAC, Patrick AFB, FL.

Booker, A. and W. Mitronovas (1964). An application of statistical discrimination to classify seismic events. *Bull. Seismolog. Soc. Amer.*, **54**, 951-971.

Cavanaugh, J.R., A.D.R. McQuarrie and R.H. Shumway (1993). Parametric and nonparametric discriminants for regional earthquakes and explosions. *PL-TR-93-2164*, Phillips Laboratory, Directorate of Geophysics, Air Force Materiel Command, Hanscom Air Force Base, MA 01731-3010, *ADA273807*.

Dargahi-Noubary, G.R. and P.J. Laycock (1981). Spectral ratio discriminants and information theory. *J. Time Series Analysis*, **2**, 71-86.

Dysart, P. and J.J. Pulli (1990). Regional seismic event classification at the NORESS array: Seismological measurements and the use of trained neural networks. *Bull. Seismolog. Soc. Amer.*, **80**, 1910-1933.

Fisk, M.D., H.L. Gray and G.D. McCartor (1993). Applications of generalized likelihood ratio tests to seismic event identification. *PL-TR-2221*, Phillips Laboratory, Directorate of Geophysics, Air Force Materiel Command, Hanscom Air Force Base, MA 01731-3010, *ADA279479*.

Kullback, S. (1959). *Information Theory and Statistics*. Repr. (1978), Gloucester, MA: Peter Smith.

Lachenbruch, P.A. and M.R. Mickey (1968). Estimation of error rates in discriminant analysis. *Technometrics*, **10**, 1-11.

Liggett, W.S. (1971). On the asymptotic optimality of spectral analysis for testing hypotheses about time series. *Ann. Math. Statist.*, , 1348-1358.

Pinsker, M.S. (1964). *Information and Information Stability of Random Variables and*

Processes. San Francisco: Holden-Day.

Renyi, A. (1961). On measures of entropy and information. *Proc. 4th Berkeley Symp. Math. Statist. Probability*, 1960, **1**, 546-561, Berkeley: University of California Press.

Richards, P.G., W-Y Kim and G. Ekström (1993). RMS Lg studies of underground nuclear explosions in the U.S.S.R. and the U.S. *PL-TR-93-2227*, Phillips Laboratory, Directorate of Geophysics, Air Force Materiel Command, Hanscom Air Force Base, MA 01731-3010, *ADA281016*.

Ryall, A.S., Jr. ed. (1993). The Novaya Zemlya event of 31 December 1992 and seismic identification issues. *PL-TR-93- 2160*, Phillips Laboratory, Directorate of Geophysics, Air Force Materiel Command, Hanscom Air Force Base, MA 01731-3010, *ADA271458*.

Shumway, R.H. (1982). Discriminant analysis for time series. In *Handbook of Statistics, Vol. 2, Pattern Recognition and Reduction of Dimensionality*, ed. P.R. Krishnaiah, 1-43. Amsterdam: North Holland.

Shumway, R.H. (1988). *Applied Statistical Time Series Analysis*, Chapter 5. Englewood Cliffs: Prentice-Hall.

Shumway, R.H. and R. Blandford (1974). An examination of some new and classical short period discriminants. *Seismic Data Analysis Center, Report No. TR-74-10*, P.O. Box 334, Alexandria, VA.

Shumway, R.H. and A.N. Unger (1974). Linear discriminant functions for stationary time series, *J. Amer. Statist. Assoc.*, **69**, 948-956.

Taylor, S.R., M.R. Denny, E.S. Vergino and R.E. Glaser (1989). Regional discrimination between NTS explosions and western U.S. earthquakes (1989). *Bull. Seismolog. Soc. Amer.*, **79**, 1142-1176.

Whittle, P. (1954). Estimation and information in stationary time series. *Arkiv. Matematik*, **2**, 423-434.

Zhang, T. and M. Taniguchi (1993). Discriminant analysis for stationary time series. Presented at U.S.-Japan Seminar on Statistical Time Series Analysis, Jan. 25-29, 1993, Honolulu. Preprint.

Zhang, T. and M. Taniguchi (1994). Discriminant analysis for stationary vector time series. *J. Time Series Analysis*, **15**, 117-126.

PART 2: ANALYSIS OF RIPPLE FIRED-SEISMIC SIGNALS

2.1 Echoes and Seismic Signals

Regional seismic monitoring and discrimination capabilities that are desirable under a potential Comprehensive Test Ban Treaty (CTBT) can be improved by developing algorithms and new procedures for distinguishing between earthquakes, nuclear explosions and mining explosions of various kinds. Much effort in past discrimination studies has concentrated on extracting various features of the spectrum that are characteristic of earthquakes, nuclear explosions or mine blasts.

One particular spectral feature that characterizes some mining explosions is a modulation of the spectrum introduced by a ripple-fired explosion. A ripple-fired event usually involves detonation of a number of explosions that are often regularly grouped in space and time. Such explosions, known as quarry blasts, have low magnitudes that may be close to those of nuclear explosions that one might monitor under the CTBT. A number of authors have examined various aspects of this problem and have proposed techniques for analyzing these ripple-fired seismic signals. Baumgardt and Ziegler (1988) have used averaged spectra and cepstra (see Bogert et al, 1963) to look for nulls that are characteristic of ripple-fired events at regional distances. Hedlin et al (1990) noted that periodic modulations persisted through the coda of ripple-fired events and used the time varying spectrum or spectogram as an analysis tool. They also introduced an automated procedure based on the empirical distribution of the maximum of the time varying cepstrum. Chapman et al (1992) look at spectral modulation in the time varying spectrum or sonogram introduced by some specific shot geometries and deconvolve using the complex cepstrum. Dysart and Pulli (1990) use the cepstrum as a measure of complexity for discrimination, noting that explosions generally have a more complicated cepstrum, whereas earthquakes have a less complex form.

The above approaches rely generally on spectral nulls for qualitative guidance as to whether an event is an earthquake, nuclear explosion or mine blast. In quarry blasts, such spectral nulls are introduced by ripple-firing, with the observed series composed of a signal, added and delayed by the sequence of shots, with an additive noise component. In this paper, we will take a new look at the predicted patterns in frequency and time induced by the signal and noise model for ripple-fired events. In the frequency domain, the spectrum, log spectrum and cepstrum are well known measures for assessing ripple firing. The spectrum will have nulls that define frequencies corresponding to the spacing

of the pulses and the duration of the pulse train. The log spectrum enhances the resulting frequency content over regions of low power and the cepstrum produces peaks at the frequencies present in the log spectrum, enabling one to estimate spacing delays between successive pulses and sometimes, even the duration of the sequence.

A new time domain method for identifying the duration spacing of the ripple fired pulses is introduced which uses autoregressive integrated moving average (ARIMA) modeling in conjunction with the autocorrelation and partial autocorrelation functions (ACF and PACF) to estimate the delay mechanism. After fitting the underlying series with a low-order autoregressive model, it is shown that the ripple-fired model with equal delays will induce in the residuals a peak in the PACF at the spacing of the pulses and a peak in the ACF residuals from the spacing pulse model at the duration value.

The frequency domain approach again uses the residuals from a low-order autoregressive model to isolate peaks in the cepstrum of the residuals. The main contribution here over previous methods is to look for periodicity in the log spectrum using residuals from previously fitted models rather than the underlying series where such peaks are generally obscured by the frequency response of the earth-seismometer system. Stripping the seasonal autoregressive components due to the spacing scalloping uncovers adjacent spacing at close delays that were obscured in the original spectrum.

Both the time domain and frequency domain methods use multiplicative models to approximate the spectrum of an observed process; that is, we assume an underlying spectrum, fitted by a autoregressive series of low order, multiplied by seasonal spectra corresponding to the spacing and duration parameters. Both methods are then tested on two simulated explosions with known patterns of time delays. The first pattern is completely regular in spacing whereas the second pattern has some variability in the spacings. Both methods work well in this case. Applying the methods to two Scandinavian explosions and two earthquakes leads to predicted spacings for the the explosions and to nonsignificant peaks in the earthquake population.

2.2 Frequency and Time Domain Methods

The general model for an observed series y_t that contains echoes can be written in terms of a train of observed signals that have been delayed and added, plus a noise, i.e.,

$$y_t = \sum_{j=0}^{n-1} a_j s_{t-T_j} + n_t \tag{2.1}$$

where n_t is additive noise, $T_0, T_1, \ldots, T_{n-1}$ are the time delays associated with the n arrivals generated by the ripple firing and $a_0, a_2, \ldots, a_{n-1}$ are the amplitudes of the arrivals. Often, by convention, $a_0 = 1$ and $T_0 = 0$ so that the initial signal appears with no delay and unit amplitude. A similar problem that has occurred in the past is testing for P-pP delays in long period data as by Shumway and Blandford (1978) who used a version of (2.1) with $n = 2, a_0 = 1, T_0 = 0$ to estimate the parameters a_1, the amplitude of the reflection and T_1, the P-pP delay time. The predicted spectrum $P_s(\omega)$ was derived from the Von Seggern and Blandford (1972) source theory. Earlier work of Hannan and Thomson (1974) used a likelihood approach with frequency dependent delay times.

Many kinds of multipath reflections, etc., can produce the behavior predicted by the signal model (2.1) and we shall be interested in the patterns that might be induced by regular ripple-firing of the kind expected with mining explosions. As an example, taking $T_j = jd$ and $a_j = 1$ in the model implies that we are interested primarily in a sequence of pulses of equal amplitude, occurring at $0, d, 2d, \ldots, (n-1)d$. This reduces (2.1) to the form

$$y_t = \sum_{j=0}^{n-1} s_{t-jd} + n_t, \tag{2.2}$$

where the delays are at multiples of an underlying delay d and the amplitudes are the same. This implies that there are n pulses spaced at interval d and we will refer to d as the spacing parameter and to the quantity nd as the duration of the signal. Hopefully, this might produce a good correspondence with what could be expected from a ripple-fired pulse train.

In this case, there are the two parameters d and n that must be identified, along with the spectra of the signal and noise, say $P_s(\omega)$ and $P_n(\omega)$, where ω is the frequency in cycles per unit time. Assuming that the signal and noise processes are independent, the spectrum of the output y_t should be of the form

$$P_y(\omega) = |A(\omega)|^2 P_s(\omega) + P_n(\omega), \tag{2.3}$$

where

$$|A(\omega)|^2 = \frac{sin^2(\pi\omega nd)}{sin^2(\pi\omega d)}. \tag{2.4}$$

The above shows that one should expect the underlying signal spectrum to be multiplied by a frequency response function that is periodic with frequencies proportional to d and nd. Hence, the cepstrum, which is the spectrum of the log spectrum, should show at least two peaks at delays of d and nd, corresponding to the spacing and duration of the pulse train.

To show an example, consider the contrived event in Figure 5 which was constructed using a simulated $2nd$ order autoregressive signal process, where a p^{th} order process, denoted by $AR(p)$ in this paper, is of the form

$$S_t = \sum_{j=1}^{p} \phi_j S_{t-j} + w_t, \tag{2.5}$$

with w_t is a white noise input process with variance σ^2. In Figure 5, we have taken $p = 2, \phi_1 = 1, \phi_2 = -.6, \sigma^2 = 1$, and the process has a smooth spectrum with a single peak that emulates that of an explosion. The process is modulated with a decaying exponential function of the form

$$g_t = \theta_1 t e^{\theta_2 t} \tag{2.6},$$

where $\log \theta_1 = -7, \theta_2 = .01$, producing the signal $s_t = g_t S_t$. The resulting signal is then delayed according to the model from (2.2) with no noise and $n = 5$, and $d = 8$. Hence there are five pulses, each separated by eight time points, leading to a signal with spacing 5 points and duration 40 (5×8) points. The time response of the pulses is shown in the upper left hand panel of Figure 6. The waveform on the lefthand side of Figure 5 has a form that emulates many explosions such as those found, for example, in Cavanaugh et al (1993). In the right hand half of Figure 5 is shown a process that has been delayed with irregular spacings; for example, we took $T_0 = T_1 = 8, T_2 = T_3 = 10, T_4 = 8, T_5 = 10$. The simulated explosions in Figure 5 are quite similar to the real Scandinavian explosions shown in Figure 11 and we assume that the generating procedure is reasonable. We assume implicitly a sampling rate of 40 points per second, leading to a folding frequency of 20 Hz.

Bogert et al (1962) proposed computing the cepstrum, i.e. the spectrum of the log spectrum, and looking for peaks that corresponded to periodicities in the log spectrum. The peaks might be identified with the spacing and duration of the sequence of pulses, since the logarithm of the product of the signal spectrum and the modulating function in (2.3) will be roughly proportional to

$$\log P_s(\omega) + 2 \log sin(\pi \omega n d) - 2 \log sin(\pi \omega d) \tag{2.7}$$

which displays it as the sum of the signal spectrum and two nonlinear periodic functions. To get an idea of what this should look like, we have computed the cepstrum of the regular pulse train in Figure 6 and the result shows major peaks at delays of 8 and 40 points with intermediate values at multiples of the spacing interval of 8 points. Hence the spacing (8 points) and duration ($8 \times 5 = 40$ points) appear as the major components of the cepstrum.

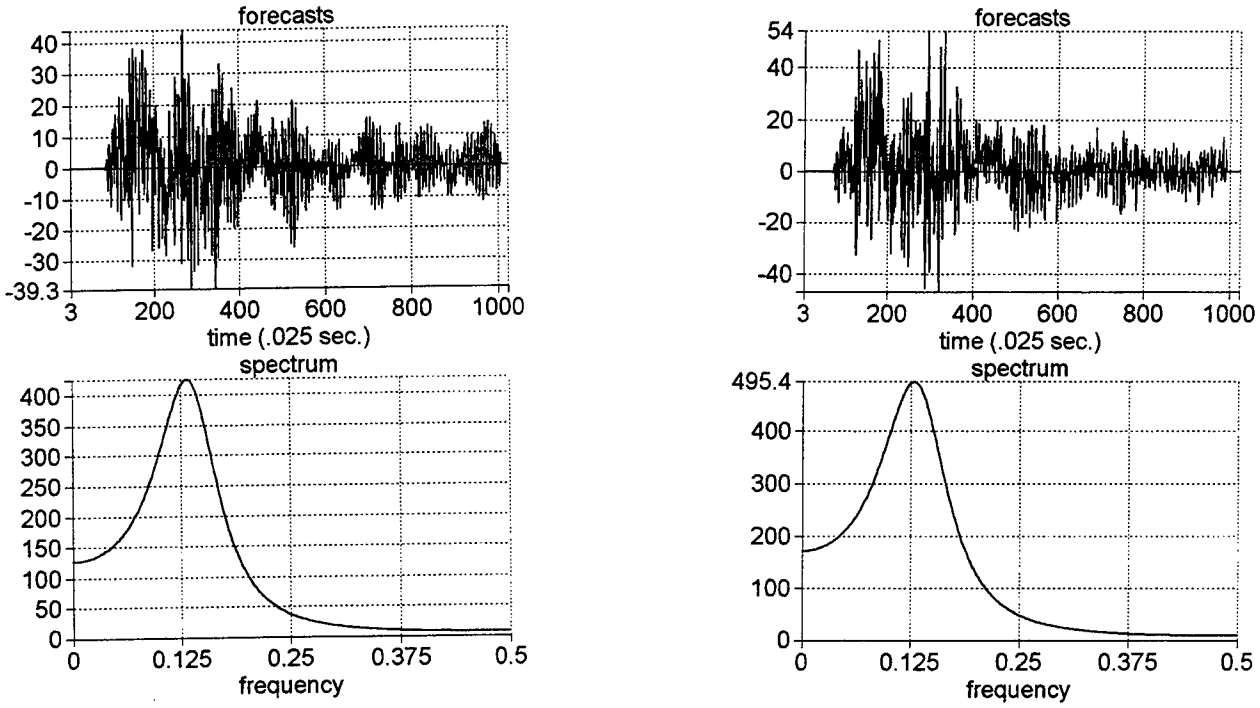

Figure 5: Simulated Series and 2nd-Order AR(2) Autoregressive Spectra. The left panel shows a simulated series formed from an echo model with $n = 5$ replicates of an AR(2) series spaced at fixed delays with spacing $d = 8$. The right panel shows the same series with $n = 6$ pulses, 2 at $d = 8$ followed by 2 at $d = 10$ followed by 1 at $d = 8$ and 1 at delay $d = 10$. Spectra measured in cycles per point (.5 cycles per point=20 Hz).

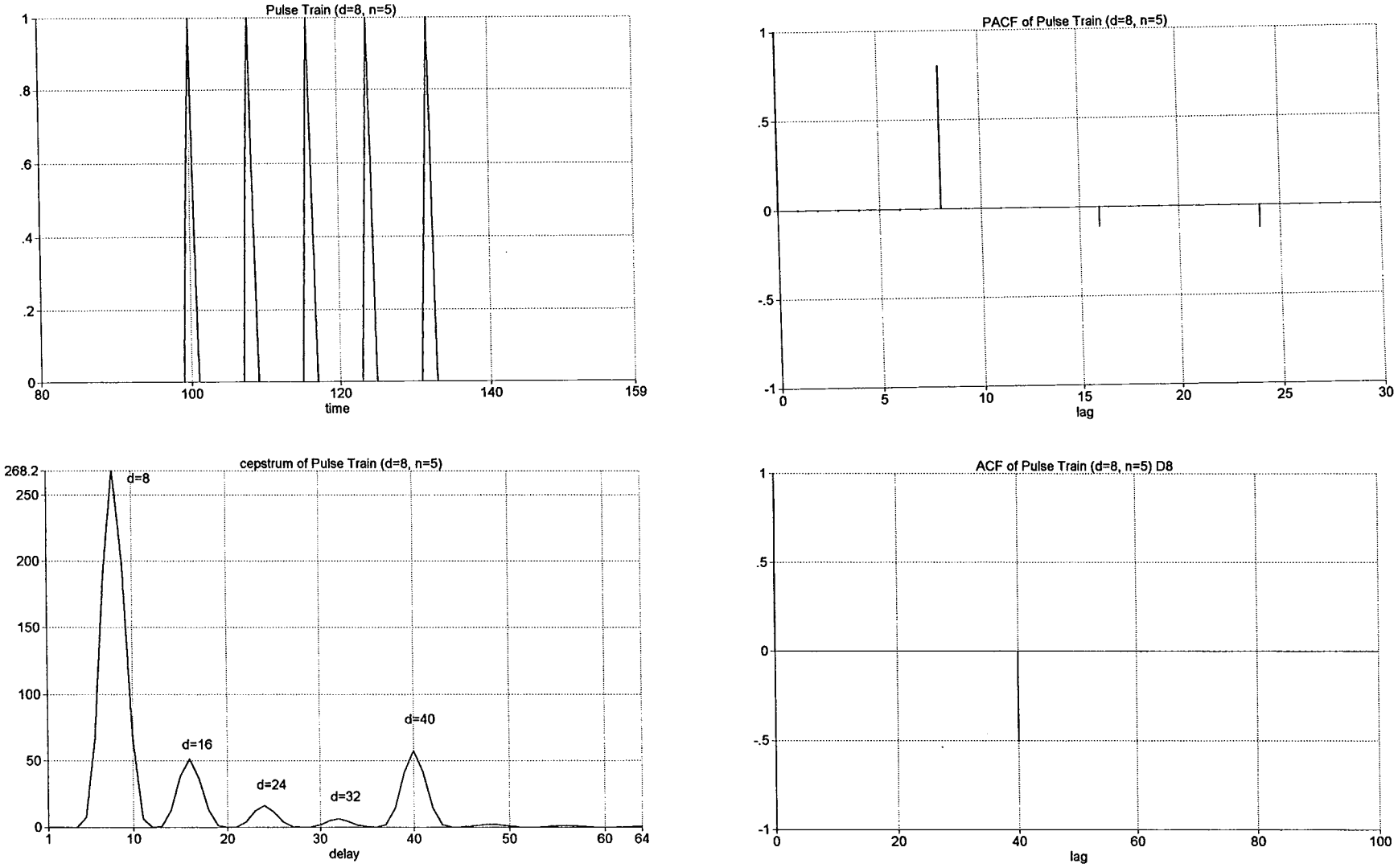

Figure 6: Theoretical Pulse Train Corresponding to the Simulated Series in the Left Panel of Figure 2.1. Also shown are the cepstrum, the PACF of the pulse train and the ACF of the seasonally differenced pulse train. Note the well defined peaks corresponding to $d = 8$ and $n = 5$ (spacing and duration of 8 and 40 points).

Significance values for peaks in the cepstrum can be approximated using the fact that the unsmoothed cepstral values are approximately distributed as a chi-squared random variable with 2 degrees of freedom. This is argued from the fact that logarithms of adjacent discrete raw spectra can be regarded as approximately Gaussian and independent so that the Fourier transforms of the same are also Gaussian. Hence, the cepstrum, as the squared Fourier transform, should have approximately a chi-squared distribution. Then, the behavior of the peak values can be compared using the fact that a chi-squared random variable with 2 degrees of freedom would be expected to exceed 3 times its theoretical value only about 5% of the time. Hence, peaks that emerge from the underlying cepstral pattern can be assumed to be significant if they are more than three times the underlying values.

An alternative time domain method that does not appear to have been tried is based on converting the signal model to an approximately equivalent time domain ARIMA process and then applying the usual diagnostic techniques. Writing the simplified model (2.2) in terms of the usual shift operator $Bs_t = s_{t-1}$ leads to

$$\begin{aligned} y_t &= \sum_{j=0}^{n-1} B^{jd} s_t + n_t \\ &= \frac{(1 - B^{nd})}{(1 - B^d)} s_t + n_t, \end{aligned} \tag{2.8}$$

which exhibits the signal part of the model as a multiplicative model with a seasonal autoregressive part with period d and a seasonal moving average part with period nd. It follows that we might look for a ratio of seasonal polynomials of the form

$$\alpha(B) = \frac{(1 - \Theta B^{nd})}{(1 - \Phi B^d)} \tag{2.9}$$

where Φ and Θ vary but may be close to one. If we assume that the underlying signal can be satisfactorily fitted with a simple autoregressive model of order p, then we might express the overall model in the multiplicative form

$$y_t = \frac{\alpha(B)}{\phi(B)} w_t \tag{2.10}$$

where

$$\phi(B) = 1 - \sum_{j=1}^{p} \phi_j B^j \tag{2.11}$$

is the autoregressive model for the modulated signal and w_t is a white noise process with variance σ^2. In general, we ignore the nonlinear modulating function g_t and concentrate on fitting a low order autoregressive model to the underlying signal first so that we estimate the polynomial $\phi(B)$ We take the order to be that suggested by the partial autocorrelation function ($PACF$) which tends to be zero after the given order. Note that one should be careful not to fit too high an order so as to obscure components of the polynomial $\alpha(B)$.

Now if one follows the usual diagnostic procedure (see, for example, Shumway, 1988), we would look at residuals from the fitted $AR(p)$, where we should see a pattern suggesting the form of $\alpha(B)$. The following pattern should be present. The PACF should have a peak at d whereas the ACF should have a peak at nd. As a practical matter, it works better to look for the peak in the PACF at d and then to fit some seasonal AR model; the ACF of the residuals from this model, say $(1 - \Phi B^d)y_t$ tend to show peaks at nd. Applying this procedure to the pulse train in Figure 6, for example, shows a well-defined peak at $d = 8$ points in the PACF of original series and a well-defined peak at $nd = 40$ points in the ACF of the residuals $(1 - B^8)y_t$. It follows that the PACF and ACF of the seasonal residuals match the pattern that would be expected for a pulse train. The cepstrum of the series of pulses shows primary peaks at $d = 8$ points and $nd = 40$ points as would be expected from the underlying model which is 5 pulses spaced by 8 points. Note also the peaks in the cepstrum at lags $8, 16$ and 32 points.

We check the diagnostic capabilities of the cepstrum and the time domain method by applying the same technique to the simulated explosions in Figure 5. In this case, the following diagnostic procedure was followed for the first simulated signal.

(i) Use the fact that the PACF in Figure 7 shows peaks at the first two lags and then a break, indicating that the underlying spectrum of the process might be satisfactorily emulated by fitting the second-order autoregressive model of the form

$$(1 - \phi_2 B - \phi_2 B^2)y_t = w_t \tag{2.12}$$

(ii) The partial autocorrelation function (PACF) of the estimated residuals $\hat{w}_t = \hat{\phi}(B)y_t$ from the above model shows a strong peak at lag 8, indicating the denominator of (2.9) holds with $d = 8$ The model now includes a seasonal autoregressive component, leading to

$$(1 - \Phi_1 B^8)(1 - \phi_2 B - \phi_2 B^2)y_t = w_t. \tag{2.13}$$

as the current proposed model. Note that we might also have included a seasonal difference term with $\Phi_1 = 1$ but some experimentation shows that the estimated

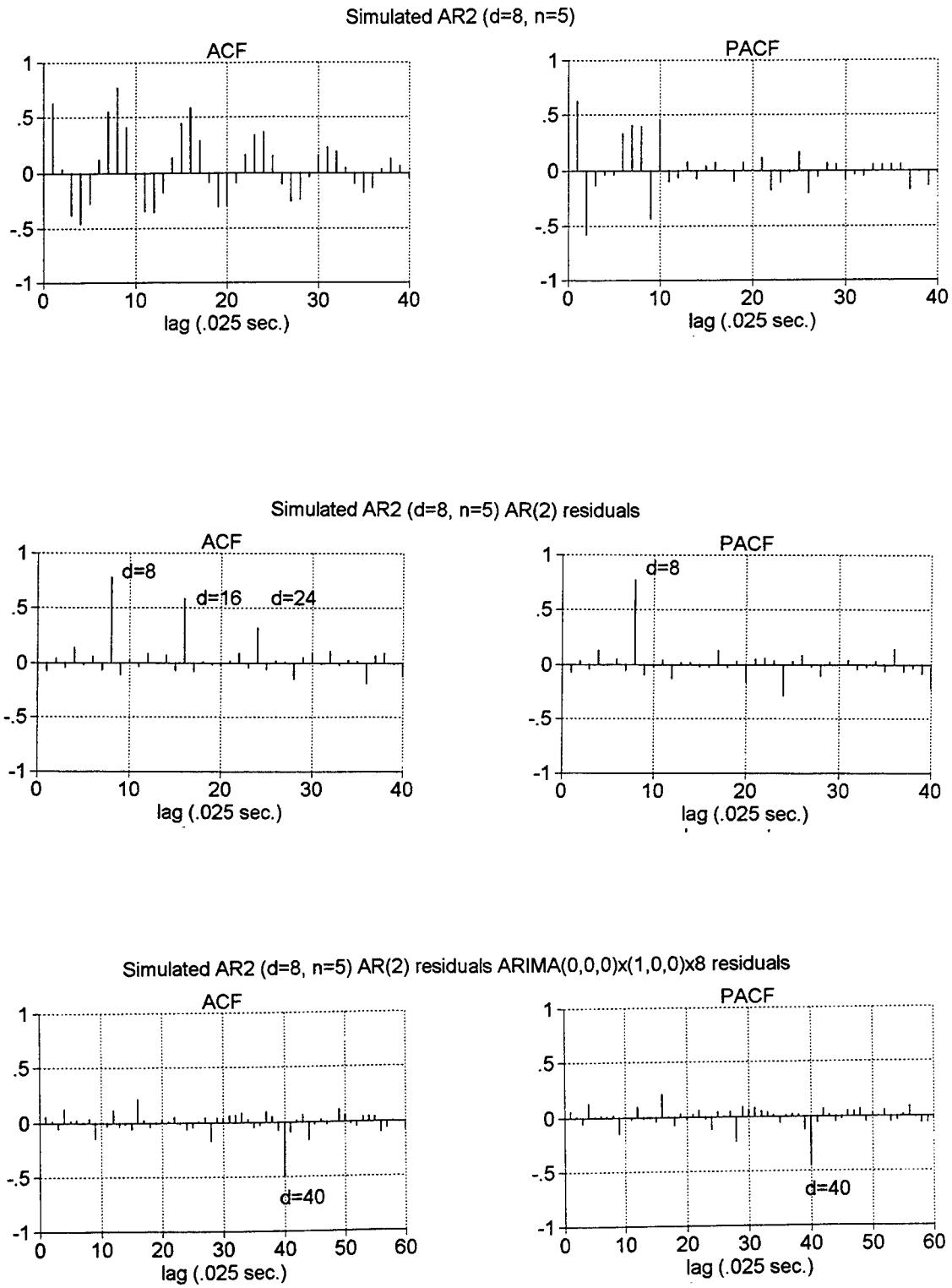

Figure 7: Autocorrelation Functions (ACF) and Partial Autocorrelation Functions (PACF) of the First Simulated Series. Top panel shows ACF and PACF of the original series; the middle panel shows ACF and PACF from residuals of the $AR(2)$ model; the bottom panel shows ACF and PACF from residuals of $SAR(8) \times AR(2)$ model. Lags are in points (1 point=.025 sec.).

values for contrived data are not that near the unit circle. Furthermore the ACF of the residuals does not exhibit the required peaks at $d, 2d, 3d, \ldots$ that would be expected for the nonstationary seasonal model.

(iii) Autocorrelations (ACF) and partial autocorrelations ($PACF$) for residuals from the model above are shown in the bottom panel of Figure 7 and they have the required peak at lag 40, indicating that $n = 5, d = 8$ are the required values for the parameters. The final model then has the seasonal moving average component with $nd = 40$, leading to the model

$$(1 - \Phi_1 B^8)(1 - \phi_2 B - \phi_2 B^2) y_t = (1 - \Theta_1 B^{40}) w_t. \tag{2.14}$$

This is not exactly the Box-Jenkins (see Shumway, 1988) form because the seasonalities on the right hand and left hand side do not match.

We note that the results for the cepstrum of the residuals $w_t = \hat{\phi}(B) y_t$, shown in Figure 8, also match almost exactly the expected forms displayed in Figure 6. The only difference in the time domain results is some additional noise in the ACF and PACF but the pattern that leads to concluding that the polynomial in (2.8) is present still persists. We conclude that the pattern generated by a fixed sequence of shots, detonated at equal spacings can be detected by either the time or frequency domain methods in this case.

For the second simulated explosion, containing irregular delays at ten points (3 delays) and at eight points (3 delays), the situation, shown in Figure 9, is somewhat more complicated. We still see the peaks at lags 1 and 2 in the $PACF$, suggesting fitting first an $AR(2)$ model as before. Residuals from this model, shown in the middle panel of Figure 9, suggest that there are delays present at 8 and 10 points, using the $PACF$. Now, fitting a seasonal $SAR(10)$ in the strongest peak leads to residuals supporting the peak at 8 points, indicating a second kind of delay. Residuals from the model with both seasonal peaks $(1 - \hat{\Phi}_2 B^8)(1 - \hat{\phi}_1 B^{10}) y_t$ do not show weak peaks at any particular duration, say $3 \times 10 + 3 \times 8 = 54$ as would be expected. The cepstrum, shown in Figure 10, shows double peaks at 8 and 10 points as well as a peak at lag 54, corresponding to the duration. There is an additional peak at the intermediate value corresponding to 28 points. Computing residuals of the form $(1 - \hat{\phi}_1 B^8)(1 - \hat{\phi}_1 B - \hat{\phi}_2 B^2) y_t$ still shows the peak at 10, 28 and 55 points.

In the next section, we apply the two single-channel single-event techniques above to two earthquakes and explosions from the Scandinavian regional event population considered by Blandford (1993) and by Cavanaugh et al (1994).

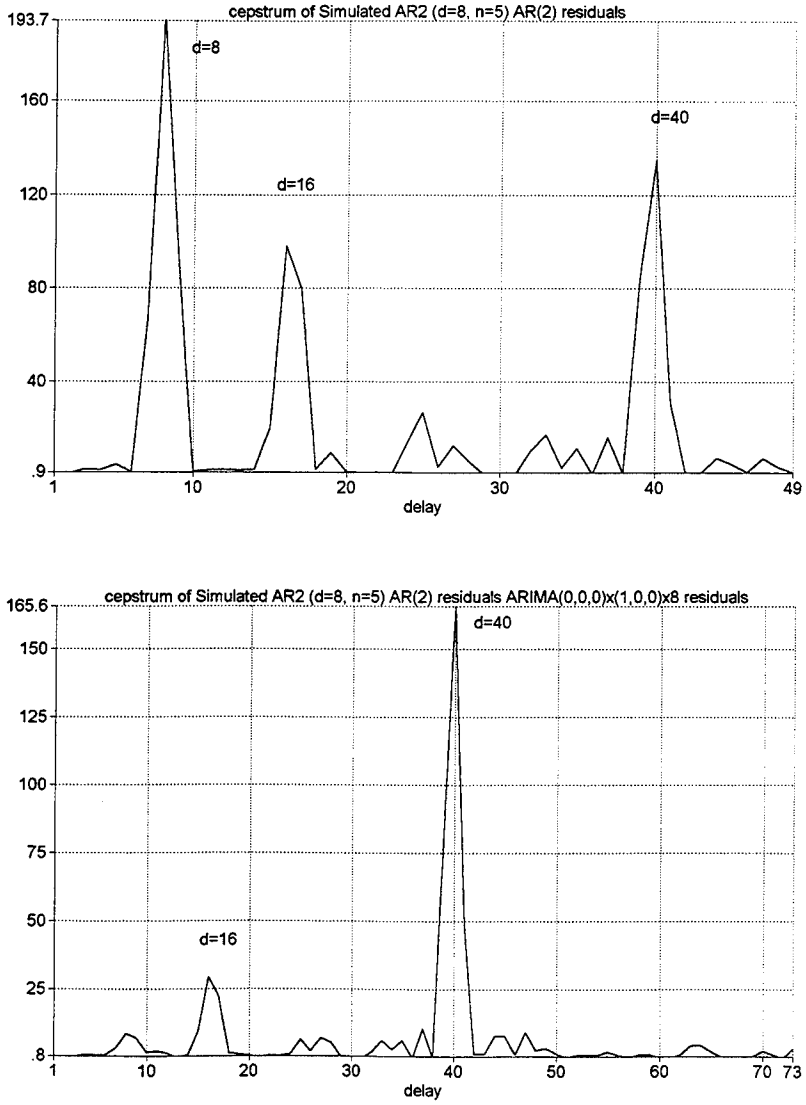

Figure 8: Cepstral Analysis of the First Simulated Series. Top panel shows cepstrum of the AR(2) residual series; bottom panel shows cepstrum of $SAR(8) \times AR(2)$ residual series. Lags are in points (1 point=.025 sec.).

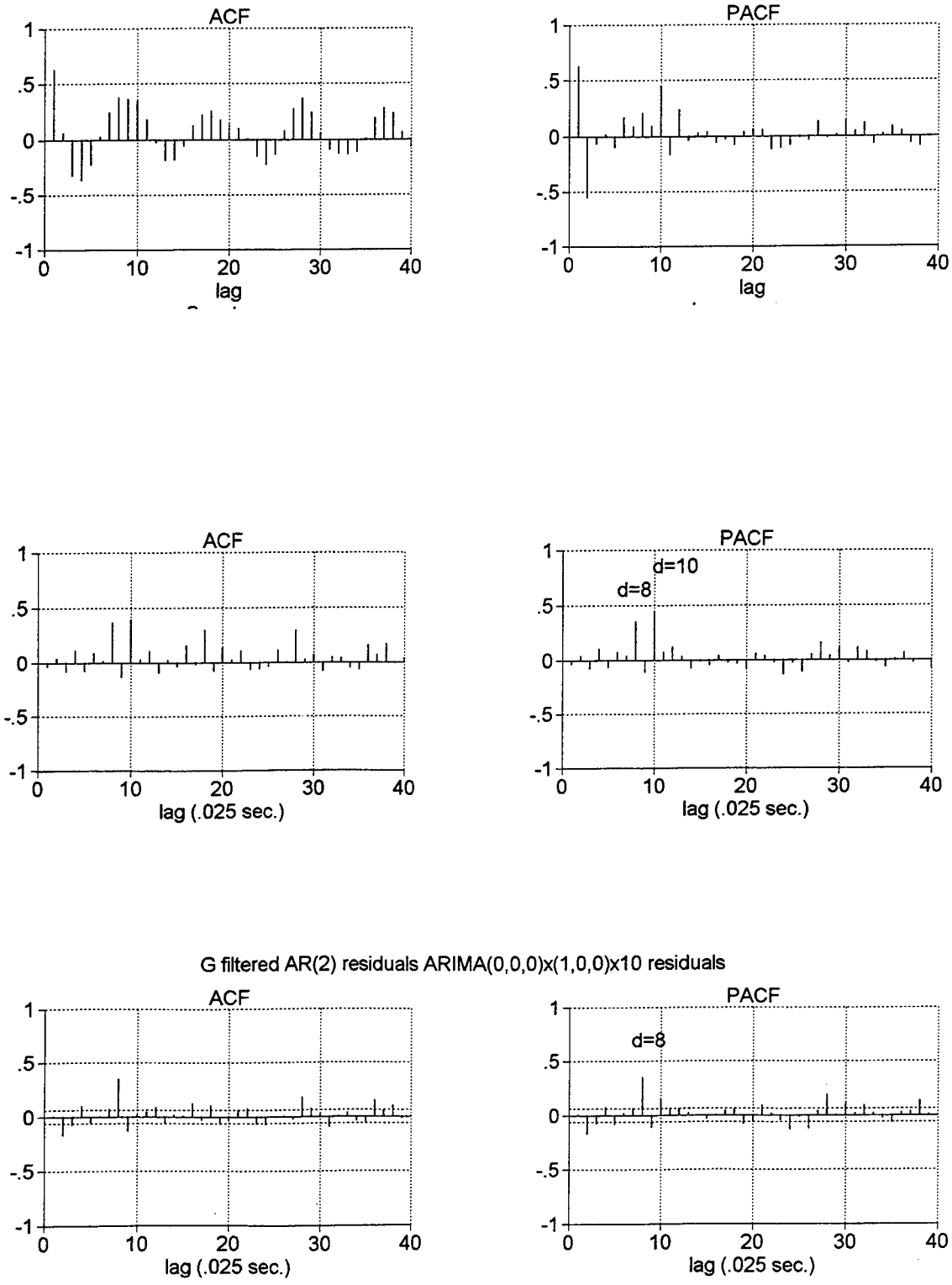

Figure 9: Autocorrelation Functions (ACF) and Partial Autocorrelation Functions (PACF) of the Second Simulated Series. Top panel shows ACF and PACF of the original series; the middle panel shows ACF and PACF from residuals of the $AR(2)$ model; the bottom panel shows ACF and PACF from residuals of $SAR(10) \times AR(2)$ model. Lags are in points (1 point=.025 sec.).

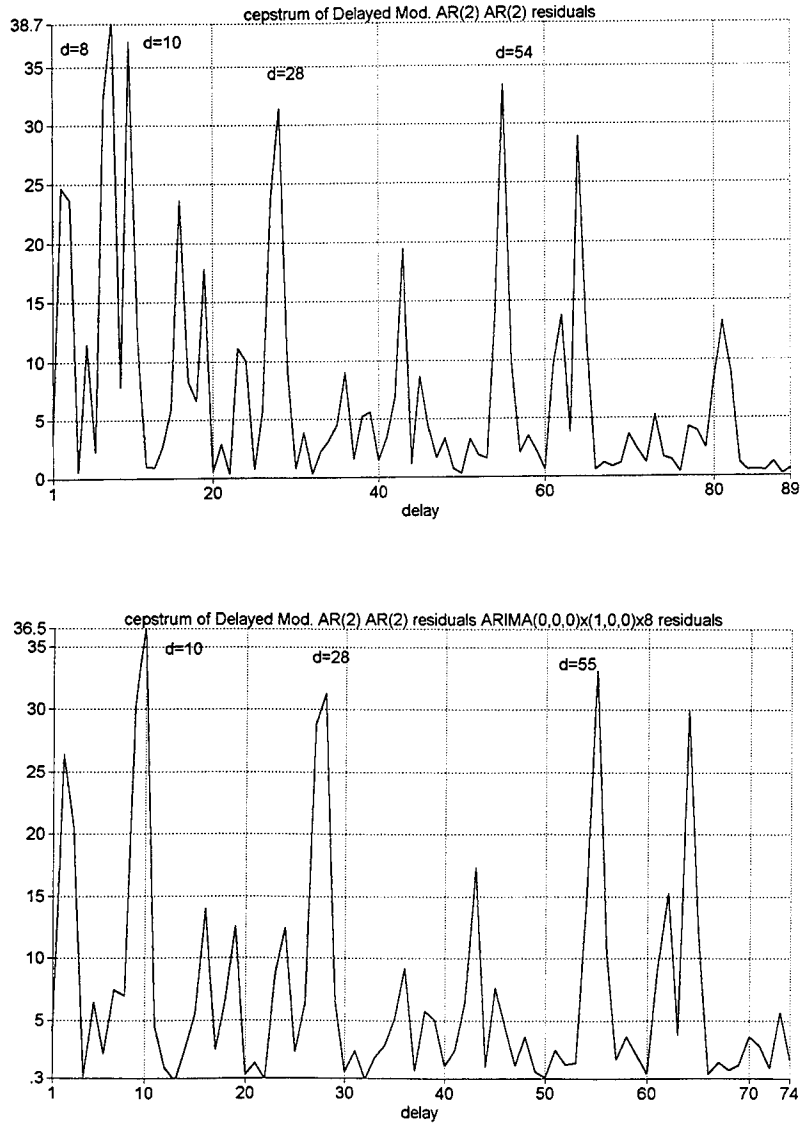

Figure 10: Cepstral Analysis of the Second Simulated Series. Top panel shows cepstrum of the $AR(2)$ residual series; bottom panel shows cepstrum of $SAR(8) \times AR(2)$ residual series. Lags are in points (1 point=.025 sec.).

2.3 Analysis of the Scandinavian Events

In order to get a sense for the structures of several typical earthquakes and explosions in the Scandinavian population, consider the two earthquakes and two explosions taken from those considered by Blandford (1993). The events chosen were two explosions (local magnitudes 2.32 and 2.59, taken from Table 1 of Blandford) and two earthquakes (local magnitudes 3.26 and 4.40 taken from Table 2 of Blandford). All events chosen by Blandford were on or near land and were distributed uniformly over Scandinavia to minimize the possibility that discriminators might be keying on location or land-sea differences. The P-phases from the two explosions and the two earthquakes are plotted in Figures 11 and 16 respectively. Note that the waveform of the second explosion, shown in the right panel of Figure 11, resembles the contrived events shown in Figure 5. We consider analyzing the two explosions, labeled 5P and 6P and the two earthquakes, labeled 5P and 6P by the methods proposed in the previous section.

(i) For the first explosion, labeled EXP 5P in Figure 11, it is necessary to first account for the primary contributor to the smooth peak part of the spectrum. Figure 12 shows the ACF and PACF of the original P-phase and it is clear from the PACF that the order of the underlying process could be taken as $p = 4$. Fitting an autoregressive $AR(4)$ model leads to the peak spectrum shown in Figure 11. The residuals from this model, given in Figure 12, have ACF and PACF showing peaks at delays $d = 17, 19$ points indicating reflections occurring at these two spacings. Fitting a seasonal $SAR(19)$ model to the $AR(4)$ residuals shows that the peak at 17 persists and we conclude tentatively that there is activity at spacings of 17 and 19 points, corresponding to about .5 seconds. The cepstral analysis in Figure 13 yields a similar conclusion. There are peaks at lag 19 and 132 points in the residual $AR(4)$ cepstrum, suggesting that a seasonal $AR(19)$ model be tried and that the duration of the pulse sequence is about 132 points or 3.3 seconds with a spacing of about .5 seconds. The duration should also appear in the PACF at lag 132 but we did not compute this due to the length of lag required. Fitting the seasonal $SAR(19)$ model uncovers a second peak at 17 points in the $AR(4) \times SAR(19)$ residuals, suggesting that there are two spacings operating in the sequence as with the simulated data analyzed in Figure 10. We conclude tentatively that there might be a pulse train of duration 3.3 seconds with pulses spaced irregularly at about .5 seconds. Note that, in this example, the ACF and PACF resolved the mixed delays on the initial examination of the $AR(4)$ residuals whereas the cepstral analysis needed to have the peak at lag 19 stripped away.

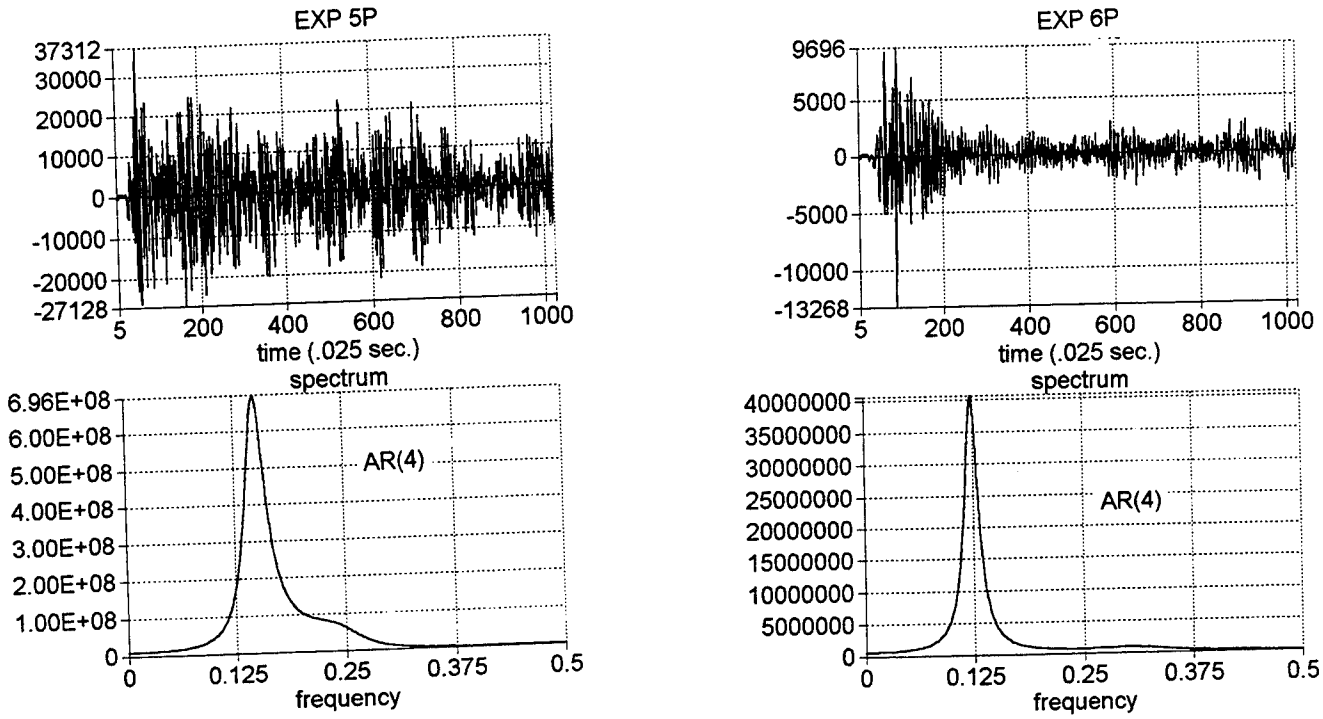

Figure 11: P-Phases From Two Scandinavian Mining Explosions and Fourth Order $AR(4)$ Autoregressive Spectra. Sampling rate is 40 points per second. Spectra measured in cycles per point (.5 cycles per point=20 Hz).

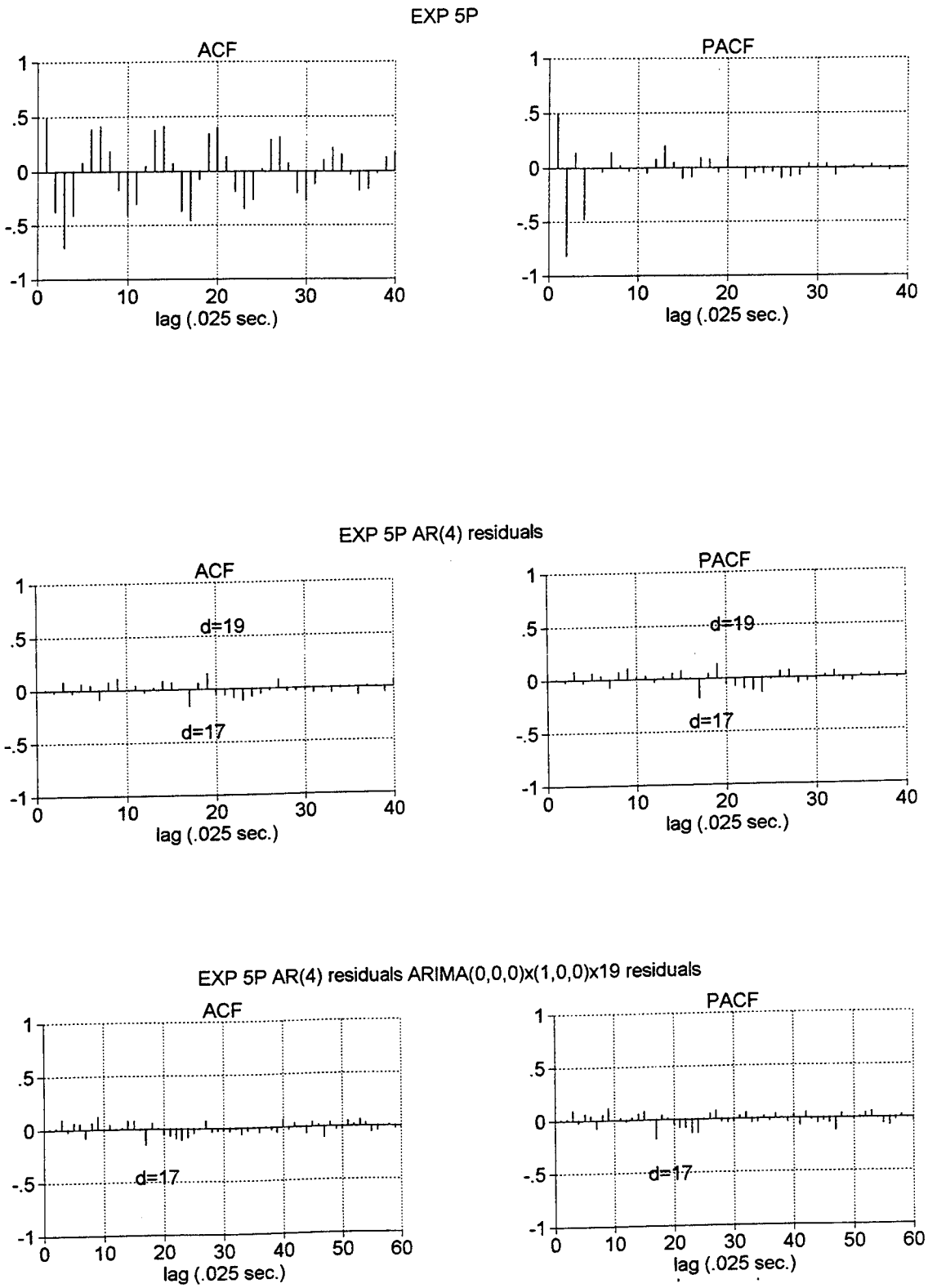

Figure 12: Autocorrelation Functions (ACF) and Partial Autocorrelation Functions (PACF) of the First Mining Explosion. Top panel shows ACF and PACF of the original series; the middle panel shows ACF and PACF from residuals of the AR(4) model; the bottom panel shows ACF and PACF from residuals of $SAR(19) \times AR(2)$ model. Lags are in points (1 point=.025 sec.)

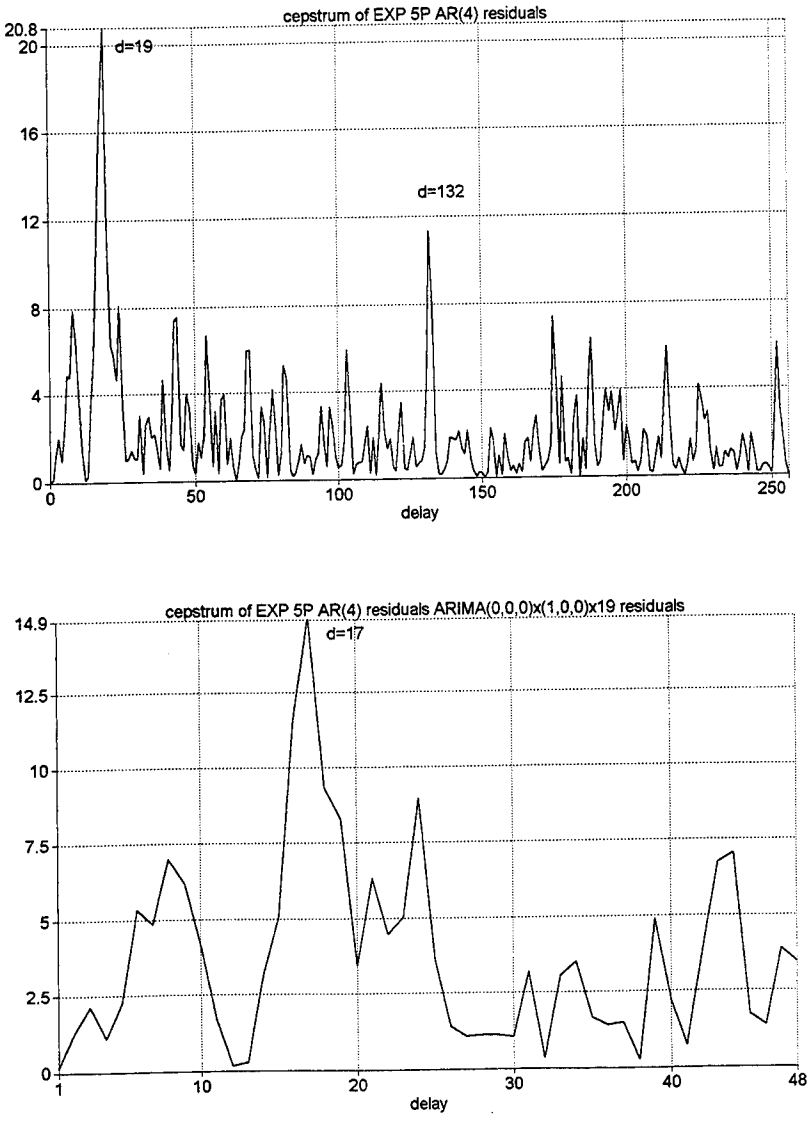

Figure 13: Cepstral Analysis of the First Mining Explosion . Top panel shows cepstrum of the AR(4) residual series; bottom panel shows cepstrum of $SAR(19) \times AR(2)$ residual series. Lags are in points (1 point=.025 sec.).

(ii) The second explosion, labeled EXP 6P in Figure 11, also was fitted reasonably well by an $AR(4)$ model since the PACF in Figure 14 is essentially zero after lag 4. Looking at the PACF (and ACF) of the $AR(4)$ residuals picks up a peak at lag 12 and we tentatively identify an $AR(4) \times SAR(12)$ model for the next step. Residuals from the above model tend to show a peak at lag 24 in the PACF, implying a $SAR(24)$ component identified with the duration of two pulses, spaced at lag 12 (.3 seconds). Looking at the cepstral analysis in Figure 15, we see first the peak at 12 in the $AR(4)$ residuals and then peaks at 12, 24, 36, 42, 57 points in the $AR(4) \times SAR(12)$ residuals. This suggests the possibility of 5 pulses spaced at about .3 seconds rather than the two pulses implied by the analysis of the ACF and PACF. Here, we note that the cepstrum seems to focus better on the pattern for the higher reflections.

(iii) The first earthquake, EQ 5P, shown in Figure 16, has substantial coefficients in the PACF, as shown in Figure 17, for lags up to 4. The $AR(4)$ spectrum shown in Figure 16 has a rather strong low frequency ripple around .125 cycles per point or 5 Hertz. Fitting a lower order $AR(2)$ to the underlying spectrum omitted the dip but did not change the conclusions below. Figure 17 shows the ACF, PACF and cepstrum of the $AR(4)$ residuals and we do not see any singular peaks in the two time domain measures or any prominent peaks in the cepstrum. The largest peak in the cepstrum at delay 7 is only about 2 times the lowest possible baseline level.

(iv) The second earthquake, EQ 6P, shown in the right hand panel of Figure 16, has a PACF, shown in Figure 18, that disappears after lag 6, implying that an $AR(6)$ model should be fitted to the underlying spectrum. The ACF, PACF and cepstrum of the $AR(6)$ residuals again do not have any particularly prominent peaks, indicating again an absence of reflections.

To conclude, we note that the explosions both displayed strong indications of reflections at equal spacings (Explosion 6P) or irregular spacings (Explosion 5P). In contrast, the two earthquakes displayed a more complex structure for the underlying signal, forcing us to fit a higher order autoregressive model for that component. The residuals, however, had a more simple pattern with no indications of reflections that might be characteristic of a ripple-fired event.

2.4 Discussion

We have developed a frequency domain method using the peaks in the cepstrum to identify the spacing and duration of echoes in a simple ripple-fired model and shown that

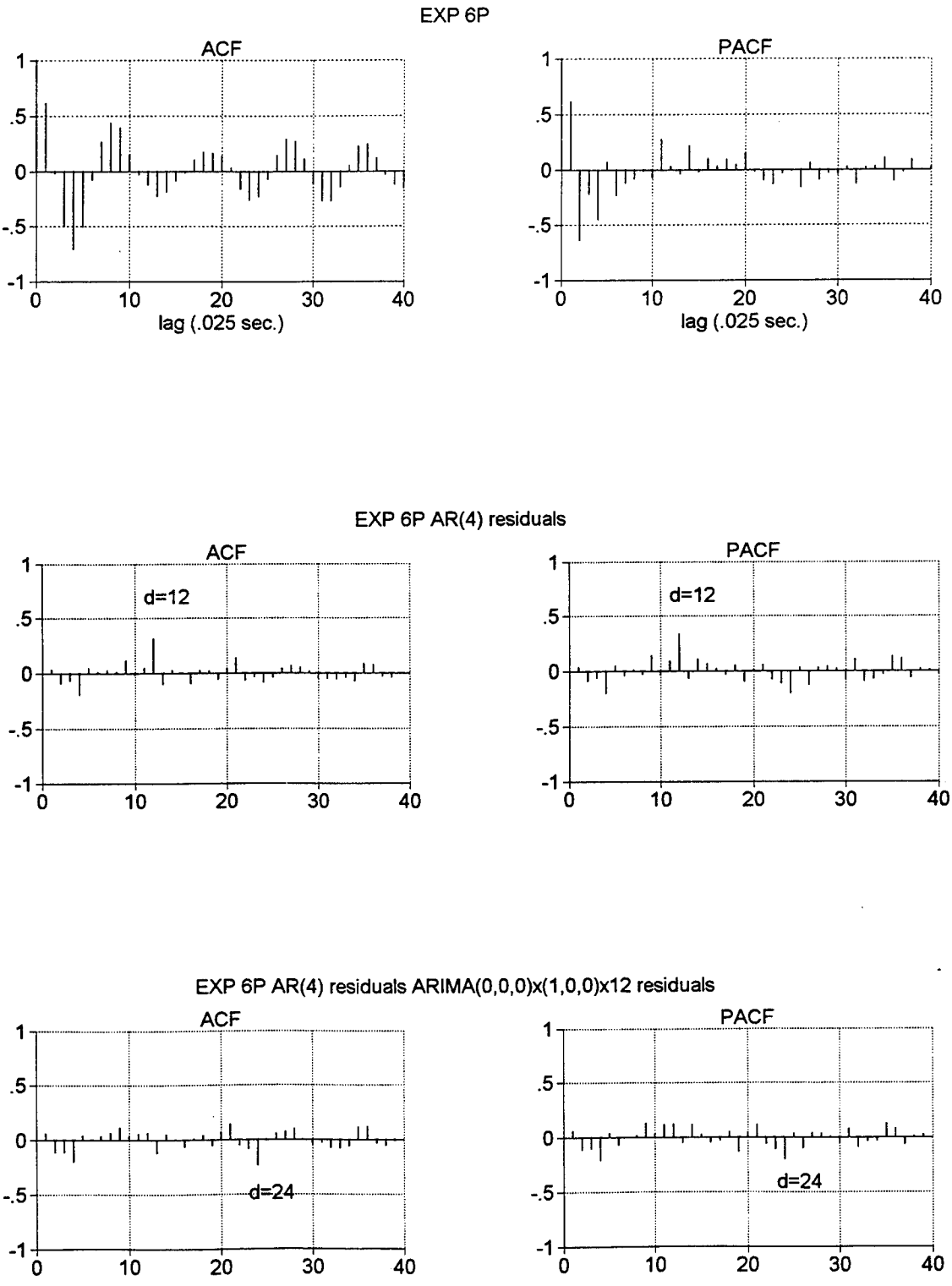

Figure 14: Autocorrelation Functions (ACF) and Partial Autocorrelation Functions (PACF) of the Second Mining Explosion. The top panel shows ACF and PACF of the original series; the middle panel shows ACF and PACF from residuals of the $AR(4)$ model; the bottom panel shows ACF and PACF from residuals of $SAR(19) \times AR(4)$ model. Lags are in points (1 point=.025 sec.).

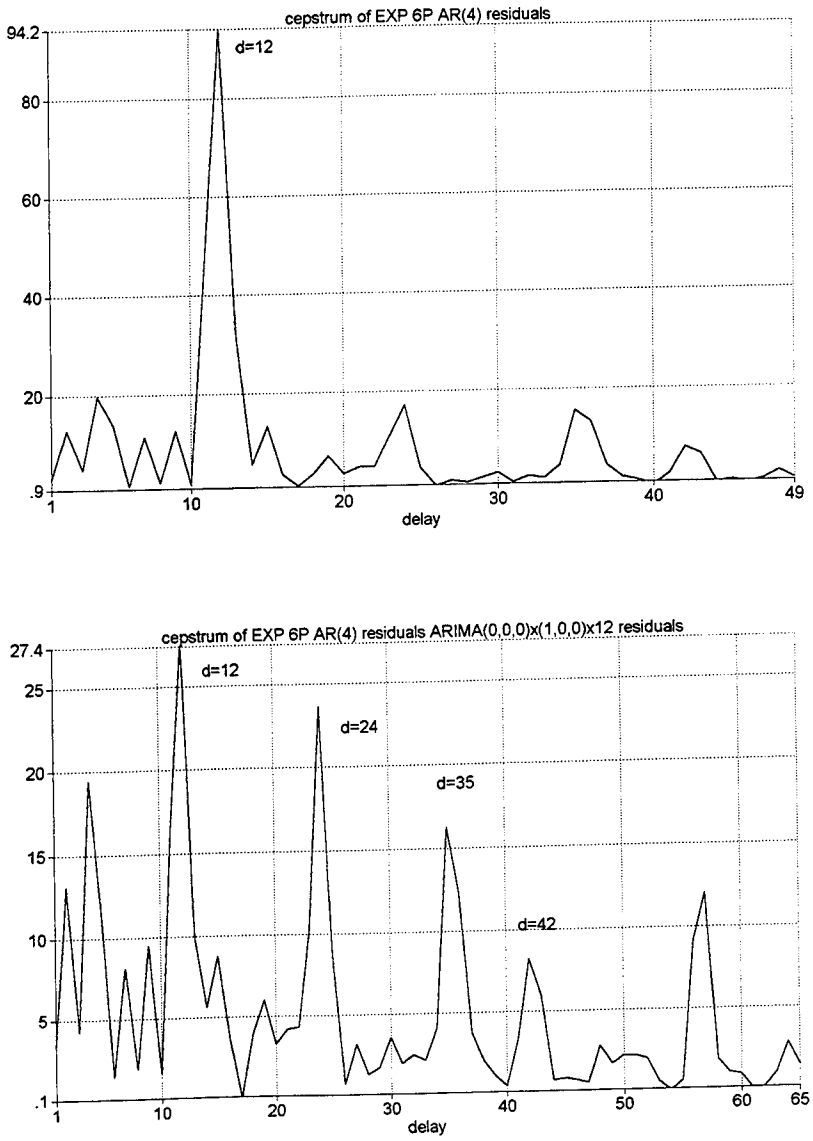

Figure 15: Cepstral Analysis of the Second Mining Explosion . The top panel shows cepstrum of the $AR(4)$ residual series; the bottom panel shows cepstrum of $SAR(12) \times AR(4)$ residual series. Lags are in points (1 point=.025 sec.).

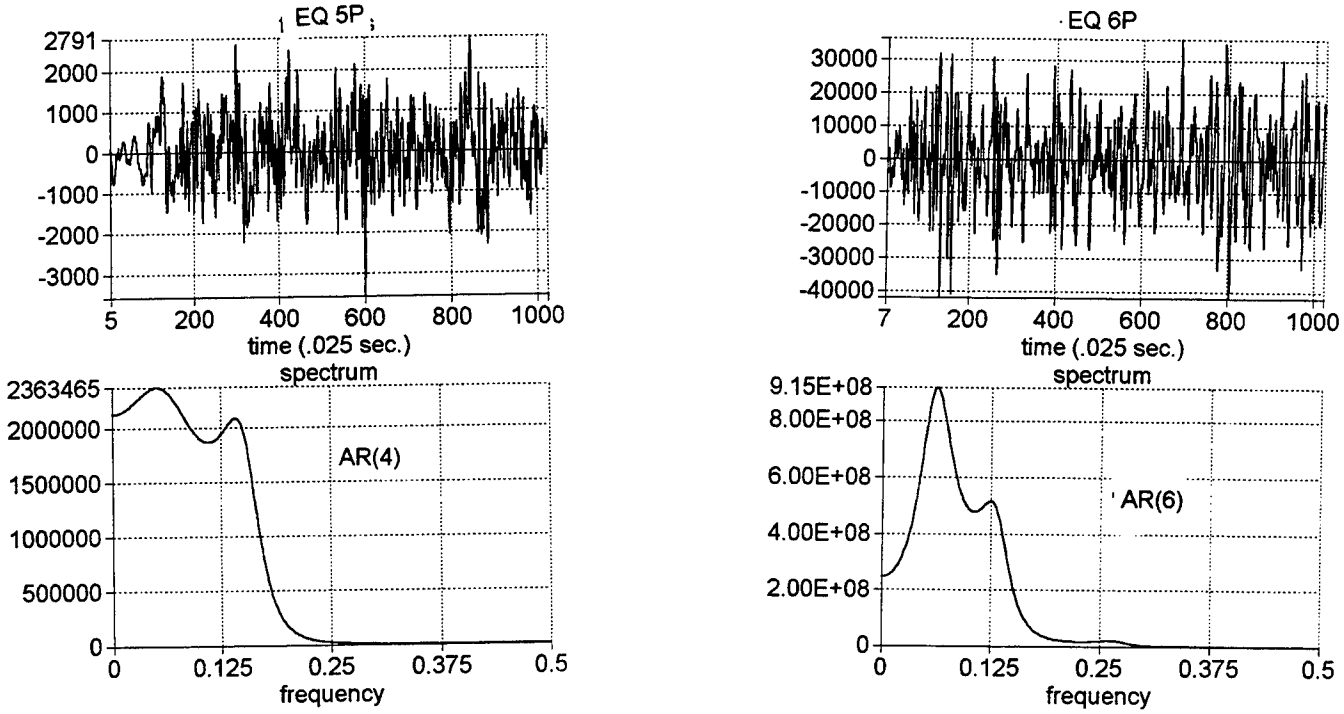

Figure 16: P-Phases From Two Scandinavian Earthquakes and Fourth Order $AR(4)$ and Sixth Order $AR(6)$ Autoregressive Spectra. Sampling rate is 40 points per second. Spectra measured in cycles per point (.5 cycles per point=20 Hz).

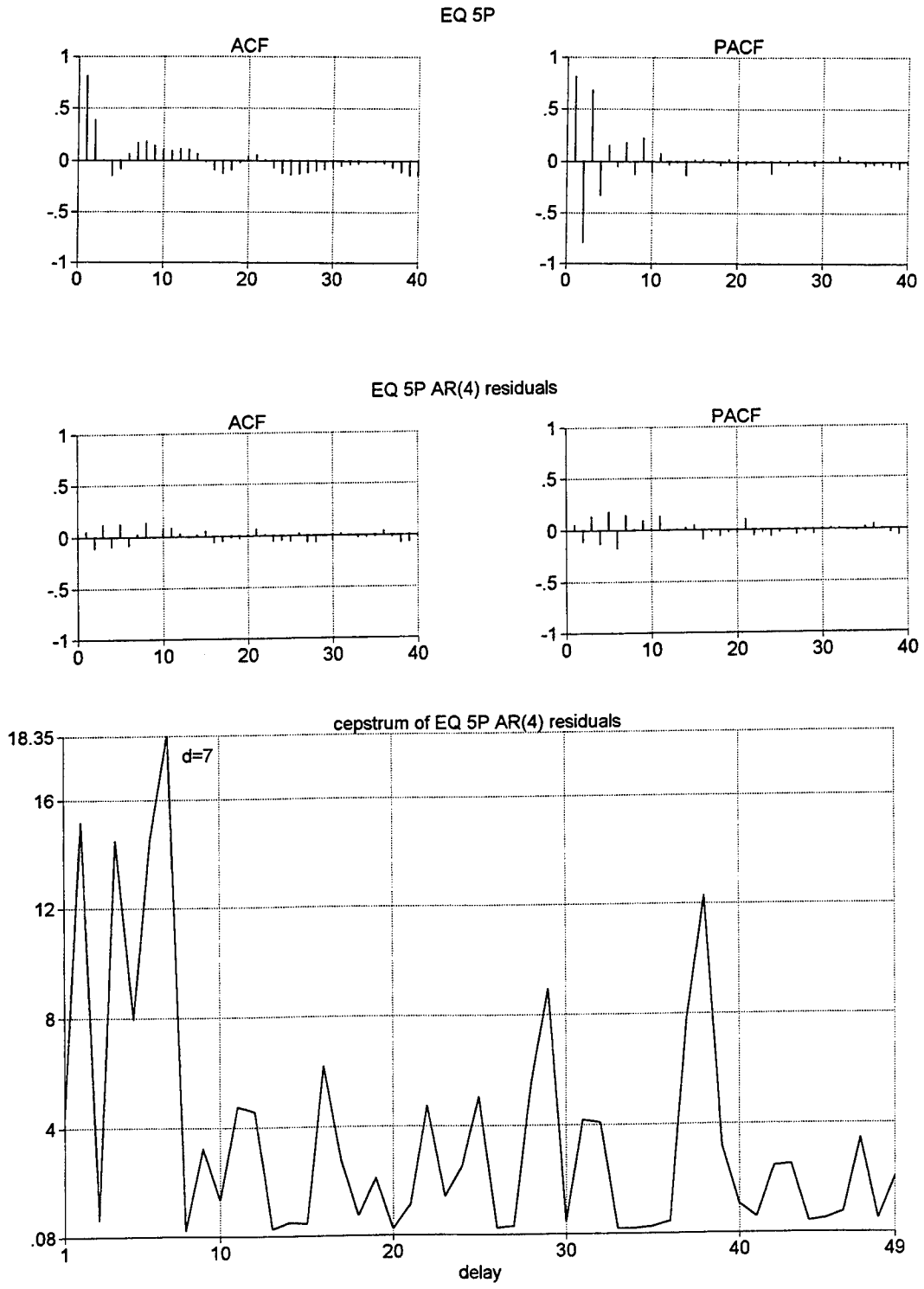

Figure 17: ACF, PACF and Cepstra of the First Earthquake. The top panel shows ACF and PACF of the original series; the middle panel shows ACF and PACF from residuals of the $AR(4)$ model; the bottom panel shows the cepstrum computed from residuals of $AR(4)$ model. Lags are in points (1 point=.025 sec.).

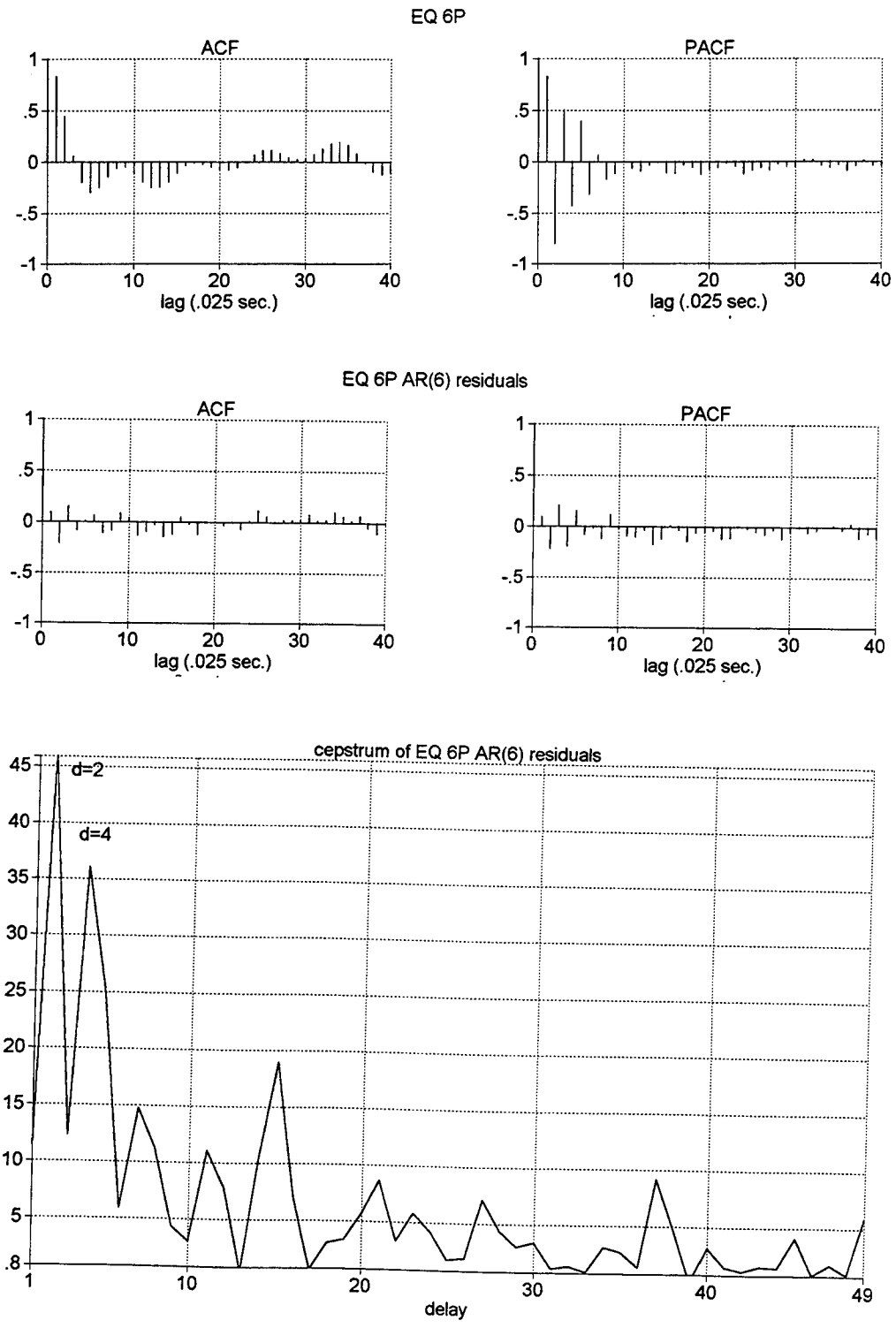

Figure 18: ACF, PACF and Cepstra of the Second Earthquake. The top panel shows ACF and PACF of the original series; the middle panel shows ACF and PACF from residuals of the $AR(6)$ model; the bottom panel shows the cepstrum computed from residuals of $AR(6)$ model. Lags are in points (1 point=.025 sec.).

it performs satisfactorily on contrived and real data. A new time domain method using the ACF and PACF to build a seasonal autoregressive moving average model for the ripple-firing phenomenon also worked well on the simulated and real data. It should be noted that the next step in the procedure should be to fit more closely some of the models implied by the identification procedures developed in this paper. That is, the diagnostic procedures can be used to suggest models of the form given in (2.2)-(2.4) in the simplest case. We need to develop methods for comparing models and for estimating the parameters n and d by maximum likelihood or some other efficient method.

To illustrate one such possible procedure, let $Y_T(\omega_k)$ denote the discrete Fourier transform of y_t, evaluated at frequencies of the form $\omega_k = 2\pi k/T, k = 0, \ldots, T-1$ and write the approximate log likelihood function

$$\log L(n,d) \propto -\sum_{k=0}^{T-1} \log P_y(\omega_k) - \sum_{k=0}^{T-1} \frac{|Y_T(\omega_k)|^2}{P_y(\omega_k)}. \tag{2.15}$$

Maximizing the above function with respect to n and d, where $P_y(\omega_k)$ is given by (2.3) and (2.4), would lead to the best fitting simple model. The approach could be extended to more irregular patterns such as that given by (2.1) since there is no particular reason why the amplitudes and time delays in (2.1) should have unit amplitudes and be equally spaced as is implied by Equation (2.2) and the arguments following it. Allowing the amplitudes $a_j, j = 0, 1, \ldots, n-1$ and time delays $T_0, T_1, \ldots, T_{n-1}$ to take general values involves adding additional parameters to the model. If general amplitudes and time delays are allowed, there is the problem of distinguishing between ripple-fired scalloping and scalloping introduced by multipath effects or by local site anomalies.

The above complications suggest that an array deconvolution approach also might be helpful. Suppose that we collect a number of explosion signals, all recorded at the same array, so that we observe the jth signal at the ith array as

$$y_{ijt} = r_{it} * s_{jt} + n_{ijt} \tag{2.16}$$

for $i = 1, 2, \ldots, r$ arrays observing $j = 1, 2, \ldots, m$ signals. The notation $*$ in (2.16) denotes convolution. The model separates effects characteristic of the site, say r_{it}, the signals s_{jt}. Shumway and Der (1984) have developed a method for simultaneously estimating the receiver functions by maximum likelihood and then deconvolving the signals. As a part of the procedure, the underlying signal spectra $P_s(\omega)$ and noise spectra $P_n(\omega)$ can be easily estimated as in Der et al (1992) so that the deconvolved signals will presumably contain only the common reflective pattern. We have not yet investigated any of the powerful capabilities of this array-based methodology.

2.5 References

Baumgardt, D.R. and K.A. Ziegler (1988). Spectral evidence for source multiplicity in explosions: Application to regional discrimination of earthquakes and explosions. *Bull. Seismolog. Soc. of Amer.*, **78**, 1773-1795.

Blandford, R.R. (1993). Discrimination of earthquakes and explosions at regional distances using complexity. *AFTAC-TR-93-044*, HQ AFTAC, Patrick AFB, FL.

Bogert, B.P., M.J.R. Healy and J.W. Tukey (1962). The frequency analysis of time series for echoes: cepstrum, pseudo-autocovariance, cross cepstrum and saphe cracking. In *Proceedings of a Symposium on Time series Analysis*, ed. M. Rosenblatt. New York: John Wiley.

Cavanaugh, J.E., A.D.R. McQuarrie and R.H. Shumway (1993) Parametric and nonparametric discriminants for regional earthquakes and explosions. *Scientific Report PL-TR-93-2164*, Phillips Laboratory, Directorate of Geophysics, Air Force Materiel Command, Hanscom AFB, MA 01731-3010, *ADA273807*.

Chapman, M.C., G.A. Bollinger and M.S. Sibol (1992). Modeling delay-fired explosion spectra and source function deconvolution at regional distances. *Final Report PL-TR-92-2250*, Phillips Laboratory, Directorate of Geophysics, Air Force Materiel Command, Hanscom Air Force Base, MA 01731-3010, ADA260232.

Der, Z.A., A.C. Lees, K.L. McLaughlin and R.H. Shumway (1992). Multichannel deconvolution of short period teleseismic and regional time series. Chapter 9 in *Statistics in the Environmental and Earth Sciences*, A.T. Walden and P. Guttorp (eds.), 156-188. London: Edward Arnold (New York: Halsted Press).

Dysart, P.S. and J.J. Pulli (1990). Regional seismic event classification at the NORESS array: Seismological measurements and the use of trained neural networks. *Bull. Seismolog. Soc. Amer.*, **80**, 1910-1933.

Hannan, E.J. and P.J. Thomson (1974). Estimating echo times. *Technometrics*, **16**, 77-84.

Hedlin, M.A.H., J.B. Minster and J.A. Orcutt (1990). An automatic means to discriminate between earthquakes and quarry blasts. *Bull. Seismolog. Soc. Amer*, **80**, 2143-2160.

Shumway, R.H. and Der, Z.A.(1985). Deconvolution of multiple time series. *Technometrics*, **27**, 385-393.

Shumway, R.H. (1988). *Applied Statistical Time Series Analysis*, Chapter 5. Englewood Cliffs: Prentice-Hall.

Shumway, R.H. and R.R. Blandford (1978). On detecting and estimating multiple arrivals from underground nuclear explosions. *SDAC-TR-77-8*, Seismic Data Analysis Center, Teledyne Geotech, 314 Montgomery St., Alexandria, VA 22314, Sponsored by the Defense Advanced Research Projects Agency.

Von Seggern, D. and R. Blandford (1972). Source time functions and spectra of underground nuclear explosions, *Geophysical J. R. Astro. Soc.*, **31**, 83-97.

Prof. Thomas Ahrens
Seismological Lab, 252-21
Division of Geological & Planetary Sciences
California Institute of Technology
Pasadena, CA 91125

Prof. Keiiti Aki
Center for Earth Sciences
University of Southern California
University Park
Los Angeles, CA 90089-0741

Prof. Shelton Alexander
Geosciences Department
403 Deike Building
The Pennsylvania State University
University Park, PA 16802

Prof. Charles B. Archambeau
University of Colorado
JSPC
Campus Box 583
Boulder, CO 80309

Dr. Thomas C. Bache, Jr.
Science Applications Int'l Corp.
10260 Campus Point Drive
San Diego, CA 92121 (2 copies)

Prof. Muawia Barazangi
Cornell University
Institute for the Study of the Continent
3126 SNEE Hall
Ithaca, NY 14853

Dr. Jeff Barker
Department of Geological Sciences
State University of New York
at Binghamton
Vestal, NY 13901

Dr. Douglas R. Baumgardt
ENSCO, Inc
5400 Port Royal Road
Springfield, VA 22151-2388

Dr. Susan Beck
Department of Geosciences
Building #77
University of Arizona
Tuscon, AZ 85721

Dr. T.J. Bennett
S-CUBED
A Division of Maxwell Laboratories
11800 Sunrise Valley Drive, Suite 1212
Reston, VA 22091

Dr. Robert Blandford
AFTAC/TT, Center for Seismic Studies
1300 North 17th Street
Suite 1450
Arlington, VA 22209-2308

Dr. Stephen Bratt
ARPA/NMRO
3701 North Fairfax Drive
Arlington, VA 22203-1714

Dale Breding
U.S. Department of Energy
Recipient, IS-20, GA-033
Office of Arms Control
Washington, DC 20585

Dr. Lawrence Burdick
C/O Barbara Wold
Dept of Biology
CA Inst. of Technology
Pasadena, CA 91125

Dr. Robert Burridge
Schlumberger-Doll Research Center
Old Quarry Road
Ridgefield, CT 06877

Dr. Jerry Carter
Center for Seismic Studies
1300 North 17th Street
Suite 1450
Arlington, VA 22209-2308

Dr. Martin Chapman
Department of Geological Sciences
Virginia Polytechnical Institute
21044 Derring Hall
Blacksburg, VA 24061

Mr Robert Cockerham
Arms Control & Disarmament Agency
320 21st Street North West
Room 5741
Washington, DC 20451,

Prof. Vernon F. Cormier
Department of Geology & Geophysics
U-45, Room 207
University of Connecticut
Storrs, CT 06268

Prof. Steven Day
Department of Geological Sciences
San Diego State University
San Diego, CA 92182

Dr. Zoltan Der
ENSCO, Inc.
5400 Port Royal Road
Springfield, VA 22151-2388

Dr. Stanley K. Dickinson
AFOSR/NM
110 Duncan Avenue
Suite B115
Bolling AFB, DC 20332-6448

Prof. Adam Dziewonski
Hoffman Laboratory, Harvard University
Dept. of Earth Atmos. & Planetary Sciences
20 Oxford Street
Cambridge, MA 02138

Prof. John Ebel
Department of Geology & Geophysics
Boston College
Chestnut Hill, MA 02167

Dr. Petr Firbas
Institute of Physics of the Earth
Masaryk University Brno
Jecna 29a
612 46 Brno, Czech Republic

Dr. Mark D. Fisk
Mission Research Corporation
735 State Street
P.O. Drawer 719
Santa Barbara, CA 93102

Prof. Donald Forsyth
Department of Geological Sciences
Brown University
Providence, RI 02912

Dr. Cliff Frolich
Institute of Geophysics
8701 North Mopac
Austin, TX 78759

Dr. Holly Given
IGPP, A-025
Scripps Institute of Oceanography
University of California, San Diego
La Jolla, CA 92093

Dr. Jeffrey W. Given
SAIC
10260 Campus Point Drive
San Diego, CA 92121

Dr. Dale Glover
Defense Intelligence Agency
ATTN: ODT-1B
Washington, DC 20301

Dr. Indra N. Gupta
Multimax, Inc.
1441 McCormick Drive
Landover, MD 20785

Dan N. Hagedon
Pacific Northwest Laboratories
Battelle Boulevard
Richland, WA 99352

Dr. James Hannon
Lawrence Livermore National Laboratory
P.O. Box 808, L-205
Livermore, CA 94550

Dr. Roger Hansen
University of Colorado, JSPC
Campus Box 583
Boulder, CO 80309

Prof. David G. Harkrider
Division of Geological & Planetary Sciences
California Institute of Technology
Pasadena, CA 91125

Prof. Danny Harvey
University of Colorado, JSPC
Campus Box 583
Boulder, CO 80309

Prof. Donald V. Helmberger
Division of Geological & Planetary Sciences
California Institute of Technology
Pasadena, CA 91125

Prof. Eugene Herrin
Geophysical Laboratory
Southern Methodist University
Dallas, TX 75275

Prof. Robert B. Herrmann
Department of Earth & Atmospheric Sciences
St. Louis University
St. Louis, MO 63156

Prof. Lane R. Johnson
Seismographic Station
University of California
Berkeley, CA 94720

Prof. Thomas H. Jordan
Department of Earth, Atmospheric &
Planetary Sciences
Massachusetts Institute of Technology
Cambridge, MA 02139

Prof. Alan Kafka
Department of Geology & Geophysics
Boston College
Chestnut Hill, MA 02167

Robert C. Kemerait
ENSCO, Inc.
445 Pineda Court
Melbourne, FL 32940

U.S. Dept of Energy
Max Koontz, NN-20, GA-033
Office of Research and Develop.
1000 Independence Avenue
Washington, DC 20585

Dr. Richard LaCoss
MIT Lincoln Laboratory, M-200B
P.O. Box 73
Lexington, MA 02173-0073

Dr. Fred K. Lamb
University of Illinois at Urbana-Champaign
Department of Physics
1110 West Green Street
Urbana, IL 61801

Prof. Charles A. Langston
Geosciences Department
403 Deike Building
The Pennsylvania State University
University Park, PA 16802

Jim Lawson, Chief Geophysicist
Oklahoma Geological Survey
Oklahoma Geophysical Observatory
P.O. Box 8
Leonard, OK 74043-0008

Prof. Thorne Lay
Institute of Tectonics
Earth Science Board
University of California, Santa Cruz
Santa Cruz, CA 95064

Dr. William Leith
U.S. Geological Survey
Mail Stop 928
Reston, VA 22092

Mr. James F. Lewkowicz
Phillips Laboratory/GPE
29 Randolph Road
Hanscom AFB, MA 01731-3010(2 copies)

Prof. L. Timothy Long
School of Geophysical Sciences
Georgia Institute of Technology
Atlanta, GA 30332

Dr. Randolph Martin, III
New England Research, Inc.
76 Olcott Drive
White River Junction, VT 05001

Dr. Robert Masse
Denver Federal Building
Box 25046, Mail Stop 967
Denver, CO 80225

Dr. Gary McCartor
Department of Physics
Southern Methodist University
Dallas, TX 75275

Prof. Thomas V. McEvilly
Seismographic Station
University of California
Berkeley, CA 94720

Dr. Art McGarr
U.S. Geological Survey
Mail Stop 977
U.S. Geological Survey
Menlo Park, CA 94025

Dr. Keith L. McLaughlin
S-CUBED
A Division of Maxwell Laboratory
P.O. Box 1620
La Jolla, CA 92038-1620

Stephen Miller & Dr. Alexander Florence
SRI International
333 Ravenswood Avenue
Box AF 116
Menlo Park, CA 94025-3493

Prof. Bernard Minster
IGPP, A-025
Scripps Institute of Oceanography
University of California, San Diego
La Jolla, CA 92093

Prof. Brian J. Mitchell
Department of Earth & Atmospheric Sciences
St. Louis University
St. Louis, MO 63156

Mr. Richard J. Morrow
USACDA/IVI
320 21st St. N.W.
Washington , DC 20451

Mr. Jack Murphy
S-CUBED
A Division of Maxwell Laboratory
11800 Sunrise Valley Drive, Suite 1212
Reston, VA 22091 (2 Copies)

Dr. Keith K. Nakanishi
Lawrence Livermore National Laboratory
L-025
P.O. Box 808
Livermore, CA 94550

Prof. John A. Orcutt
IGPP, A-025
Scripps Institute of Oceanography
University of California, San Diego
La Jolla, CA 92093

Prof. Jeffrey Park
Kline Geology Laboratory
P.O. Box 6666
New Haven, CT 06511-8130

Dr. Howard Patton
Lawrence Livermore National Laboratory
L-025
P.O. Box 808
Livermore, CA 94550

Dr. Frank Pilotte
HQ AFTAC/TT
1030 South Highway A1A
Patrick AFB, FL 32925-3002

Dr. Jay J. Pulli
Radix Systems, Inc.
201 Perry Parkway
Gaithersburg, MD 20877

Dr. Robert Reinke
ATTN: FCTVTD
Field Command
Defense Nuclear Agency
Kirtland AFB, NM 87115

Prof. Paul G. Richards
Lamont-Doherty Earth Observatory
of Columbia University
Palisades, NY 10964

Mr. Wilmer Rivers
Teledyne Geotech
1300 17th St N #1450
Arlington, VA 22209-3803

Dr. Alan S. Ryall, Jr.
ARPA/NMRO
3701 North Fairfax Drive
Arlington, VA 22203-1714

Dr.Chandan K. Saikia
Woodward Clyde- Consultants
566 El Dorado Street
Pasadena, CA 91101

Dr. Richard Sailor
TASC, Inc.
55 Walkers Brook Drive
Reading, MA 01867

Prof. Charles G. Sammis
Center for Earth Sciences
University of Southern California
University Park
Los Angeles, CA 90089-0741

Prof. Christopher H. Scholz
Lamont-Doherty Earth Observatory
of Columbia University
Palisades, NY 10964

Dr. Susan Schwartz
Institute of Tectonics
1156 High Street
Santa Cruz, CA 95064

Mr. Dogan Seber
Cornell University
Inst. for the Study of the Continent
3130 SNEE Hall
Ithaca, NY 14853-1504

Secretary of the Air Force
(SAFRD)
Washington, DC 20330

Office of the Secretary of Defense
DDR&E
Washington, DC 20330

Thomas J. Sereno, Jr.
Science Application Int'l Corp.
10260 Campus Point Drive
San Diego, CA 92121

Dr. Michael Shore
Defense Nuclear Agency/SPSS
6801 Telegraph Road
Alexandria, VA 22310

Dr. Robert Shumway
University of California Davis
Division of Statistics
Davis, CA 95616

Dr. Matthew Sibol
Virginia Tech
Seismological Observatory
4044 Derring Hall
Blacksburg, VA 24061-0420

Prof. David G. Simpson
IRIS, Inc.
1616 North Fort Myer Drive
Suite 1050
Arlington, VA 22209

Donald L. Springer
Lawrence Livermore National Laboratory
L-025
P.O. Box 808
Livermore, CA 94550

Dr. Jeffrey Stevens
S-CUBED
A Division of Maxwell Laboratory
P.O. Box 1620
La Jolla, CA 92038-1620

Prof. Brian Stump
Los Alamos National Laboratory
EES-3
Mail Stop C-335
Los Alamos, NM 87545

Prof. Jeremiah Sullivan
University of Illinois at Urbana-Champaign
Department of Physics
1110 West Green Street
Urbana, IL 61801

Prof. L. Sykes
Lamont-Doherty Earth Observatory
of Columbia University
Palisades, NY 10964

Dr. David Taylor
ENSCO, Inc.
445 Pineda Court
Melbourne, FL 32940

Dr. Steven R. Taylor
Los Alamos National Laboratory
P.O. Box 1663
Mail Stop C335
Los Alamos, NM 87545

Prof. Tuncay Taymaz
Istanbul Technical University
Dept. of Geophysical Engineering
Mining Faculty
Maslak-80626, Istanbul Turkey

Prof. Clifford Thurber
University of Wisconsin-Madison
Department of Geology & Geophysics
1215 West Dayton Street
Madison, WS 53706

Prof. M. Nafi Toksoz
Earth Resources Lab
Massachusetts Institute of Technology
42 Carleton Street
Cambridge, MA 02142

Dr. Larry Turnbull
CIA-OSWR/NED
Washington, DC 20505

Dr. Gregory van der Vink
IRIS, Inc.
1616 North Fort Myer Drive
Suite 1050
Arlington, VA 22209

Dr. Karl Veith
EG&G
5211 Auth Road
Suite 240
Suitland, MD 20746

Prof. Terry C. Wallace
Department of Geosciences
Building #77
University of Arizona
Tuscon, AZ 85721

Dr. Thomas Weaver
Los Alamos National Laboratory
P.O. Box 1663
Mail Stop C335
Los Alamos, NM 87545

Dr. William Wortman
Mission Research Corporation
8560 Cinderbed Road
Suite 700
Newington, VA 22122

Prof. Francis T. Wu
Department of Geological Sciences
State University of New York
at Binghamton
Vestal, NY 13901

Prof Ru-Shan Wu
University of California, Santa Cruz
Earth Sciences Department
Santa Cruz, CA 95064

ARPA, OASB/Library
3701 North Fairfax Drive
Arlington, VA 22203-1714

HQ DNA
ATTN: Technical Library
Washington, DC 20305

Defense Technical Information Center
Cameron Station
Alexandria, VA 22314 (2 Copies)

TACTEC
Battelle Memorial Institute
505 King Avenue
Columbus, OH 43201 (Final Report)

Phillips Laboratory
ATTN: XPG
29 Randolph Road
Hanscom AFB, MA 01731-3010

Phillips Laboratory
ATTN: GPE
29 Randolph Road
Hanscom AFB, MA 01731-3010

Phillips Laboratory
ATTN: TSML
5 Wright Street
Hanscom AFB, MA 01731-3004

Phillips Laboratory
ATTN: PL/SUL
3550 Aberdeen Ave SE
Kirtland, NM 87117-5776 (2 copies)

Dr. Michel Bouchon
I.R.I.G.M.-B.P. 68
38402 St. Martin D'Heres
Cedex, FRANCE

Dr. Michel Campillo
Observatoire de Grenoble
I.R.I.G.M.-B.P. 53
38041 Grenoble, FRANCE

Dr. Kin Yip Chun
Geophysics Division
Physics Department
University of Toronto
Ontario, CANADA

Prof. Hans-Peter Harjes
Institute for Geophysic
Ruhr University/Bochum
P.O. Box 102148
4630 Bochum 1, GERMANY

Prof. Eystein Husebye
NTNF/NORSAR
P.O. Box 51
N-2007 Kjeller, NORWAY

David Jepsen
Acting Head, Nuclear Monitoring Section
Bureau of Mineral Resources
Geology and Geophysics
G.P.O. Box 378, Canberra, AUSTRALIA

Ms. Eva Johannisson
Senior Research Officer
FOA
S-172 90 Sundbyberg, SWEDEN

Dr. Peter Marshall
Procurement Executive
Ministry of Defense
Blacknest, Brimpton
Reading FG7-FRS, UNITED KINGDOM

Dr. Bernard Massinon, Dr. Pierre Mechler
Societe Radiomana
27 rue Claude Bernard
75005 Paris, FRANCE (2 Copies)

Dr. Svein Mykkeltveit
NTNT/NORSAR
P.O. Box 51
N-2007 Kjeller, NORWAY (3 Copies)

Prof. Keith Priestley
University of Cambridge
Bullard Labs, Dept. of Earth Sciences
Madingley Rise, Madingley Road
Cambridge CB3 OEZ, ENGLAND

Dr. Jorg Schlittenhardt
Federal Institute for Geosciences & Nat'l Res.
Postfach 510153
D-30631 Hannover , GERMANY

Dr. Johannes Schweitzer
Institute of Geophysics
Ruhr University/Bochum
P.O. Box 1102148
4360 Bochum 1, GERMANY

Trust & Verify
VERTIC
Carrara House
20 Embankment Place
London WC2N 6NN, ENGLAND